american physiological society

JNP JOURNAL OF NEUROPHYSIOLOGY

J Neurophysiol 130: 69–85, 2023.
First published May 31, 2023; doi:10.1152/jn.00443.2022

RESEARCH ARTICLE

Cellular and Molecular Properties of Neurons

Use-dependent facilitation of electrical transmission involves changes to postsynaptic K^+ current

Yueling Gu, Kelly H. Lee, Alex B. Prosserman, and Neil S. Magoski

Department of Biomedical and Molecular Sciences, Queen's University, Kingston, Ontario, Canada

Abstract

Activity-dependent modulation of electrical transmission typically involves Ca^{2+} influx acting directly on gap junctions or initiating Ca^{2+}-dependent pathways that in turn modulate coupling. We now describe short-term use-dependent facilitation of electrical transmission between bag cell neurons from the hermaphroditic snail, *Aplysia californica*, that is instead mediated by changes in postsynaptic responsiveness. Bag cell neurons secrete reproductive hormone during a synchronous afterdischarge of action potentials coordinated by electrical coupling. Here, recordings from pairs of coupled bag cell neurons in culture showed that nonjunctional currents influence electrical transmission in a dynamic manner. Under a dual whole cell voltage-clamp, the junctional current was linear and largely voltage-independent, while in current-clamp, the coupling coefficient was similar regardless of the extent of presynaptic hyperpolarization. Moreover, a train stimulus of action potential-like waveforms, in a voltage-clamped presynaptic neuron, elicited electrotonic potentials, in a current-clamped postsynaptic neuron, that facilitated over time when delivered at a frequency approximating the afterdischarge. Junctional current remained constant over the train stimulus, as did postsynaptic voltage-gated Ca^{2+} current. However, postsynaptic voltage-gated K^+ current underwent cumulative inactivation, suggesting that K^+ current run-down facilitates the electrotonic potential by boosting the response to successive junctional currents. Accordingly, preventing run-down by blocking postsynaptic K^+ channels occluded facilitation. Finally, stimulation of bursts in coupled pairs resulted in synchronous firing, where active neurons could recruit silent partners through short-term use-dependent facilitation. Thus, potentiation of electrical transmission may promote synchrony in bag cell neurons and, by extension, reproductive function.

NEW & NOTEWORTHY The understanding of how activity can facilitate electrical transmission is incomplete. We found that electrotonic potentials between electrically coupled neuroendocrine bag cell neurons facilitated in a use-dependent fashion. Rather than changes to the junctional current, facilitation was associated with cumulative inactivation of postsynaptic K^+ current, presumably augmenting responsiveness. When made to burst, neurons synchronized their spiking, in part by use-dependent facilitation bringing quiescent cells to the threshold. Facilitation may foster en masse firing and neurosecretion.

afterdischarge; gap junction; junctional current; mollusc; neuroendocrine cell

INTRODUCTION

Electrical synapses consist of connexin (for vertebrates) or innexin (for invertebrates) protein subunits forming hemichannels that pair between adjacent neurons to make a gap junction (1–3). Electrical transmission comprises direct electrotonic signaling from presynaptic to postsynaptic neurons through gap junctions and may well engage conductances in the postsynaptic membrane (4–6). Along with synchronization, electrical transmission can allow for feedforward excitation, where an active neuron elicits spikes in a coupled partner (5). Triggering the postsynaptic cell often requires repetitive presynaptic firing, which opens up the possibility that facilitation (7) may contribute to feedforward excitation (8).

The facilitation of chemical transmission has been extensively studied (9, 10) but is less understood for electrical transmission. At leech Retzius cell and rat thalamic electrical synapses, a presynaptic burst results in Ca^{2+} entry and enhancement of the junctional conductance (11, 12), perhaps via calmodulin kinase phosphorylating hemichannels

Correspondence: N.S. Magoski (magoski@queensu.ca).
Submitted 27 October 2022 / Revised 10 May 2023 / Accepted 18 May 2023

(13). At the goldfish mixed, sensory-to-Mauthner cell synapse, the electrical component is facilitated by the chemical component opening postsynaptic, Ca^{2+}-permeable *N*-methyl D-aspartate receptors during presynaptic tetanic stimulation (14). Aside from these tetanus-induced changes, there is a lack of evidence for electrical transmission undergoing facilitation akin to short-term potentiation of chemical transmission, i.e., where the postsynaptic response becomes progressively greater during presynaptic firing (15–17). Here, we use coupled bag cell neurons from the marine mollusk, *Aplysia californica*, to demonstrate use-dependent facilitation of electrical transmission.

Ovulation in *Aplysia* is under the command of bag cell neurons, which are neuroendocrine cells that secrete egg-laying hormone over the course of a protracted action potential afterdischarge (18–20). Bag cell neurons are situated in two clusters, just rostral to the abdominal ganglion within the central nervous system (21). A cholinergic synaptic input from higher brain areas, lasting only a few seconds, causes the neurons to depolarize from ~−60 to ~−40 mV, with the afterdischarge then proceeding in two phases of firing: an ~1-min, 5-Hz fast phase, followed by an ~30-min, 1-Hz slow phase (22–24). Action potentials during the fast-phase peak at ~+30 mV with an ~40-ms half-width, whereas for the slow-phase they reach ~+40 mV and are ~60 ms wide (23). Intra- and inter-cluster electrical couplings guarantee that the neurons fire in synchrony so as to release the hormone, primarily during the slow phase, at a nearby neurohemal area (25–29). Gap junctions also appear to support the spatial spread of excitation within and between clusters (30, 31).

The present study shows that during slow-phase-like stimulation (1 Hz), but not fast-phase-like (5 Hz), the electrotonic potential facilitates and can lead to feedforward excitation. Moreover, instead of potentiating junctional conductance, repetitive stimulation enhances postsynaptic excitability, and this is mirrored by a cumulative inactivation of K^+ channels. Electrical coupling is employed by neuroendocrine systems in the adrenal medulla and hypothalamus to achieve synchronization (32–34). For bag cell neurons, use-dependent facilitation of electrical transmission could sustain the uniform activity necessary for collective hormone release.

METHODS

Animals and Cell Culture

Specimens of the hermaphrodite *A. californica* weighing 150–500 g were obtained from Marinus (Lakewood, CA) and housed in an ~300-L aquarium containing continuously circulating, aerated seawater (Instant Ocean; Aquarium Systems; Mentor, OH) at 16–18°C on a 12:12-h light/dark cycle, and fed romaine lettuce 6–7 times/wk. All experiments were approved by the Queen's University Animal Care Committee (protocols Magoski-1501 or Magoski-1745).

For primary cultures of isolated bag cell neurons, animals were anesthetized by an injection of isotonic $MgCl_2$ (390 mM; volume ~50% of body wt), the abdominal ganglion was removed and treated for 18 h at 22°C with Dispase II (13.3 mg/mL; 4942078001; Roche/Sigma-Aldrich, Oakville, ON, Canada) dissolved in tissue culture artificial seawater (tcASW) [composition in mM: 460 NaCl, 10.4 KCl, 11 $CaCl_2$, 55 $MgCl_2$, 15 N-2-hydroxyethylpiperazine-N'-2-ethanesulphonic acid (HEPES), 1 mg/mL glucose, and 100 U/mL penicillin plus 0.1 mg/mL streptomycin (P4333; Sigma-Aldrich), pH 7.8 with NaOH]. The remainder of the nervous system was also removed to achieve euthanasia. After enzyme treatment, the ganglion was rinsed in tcASW for 1 h, and fine scissors and forceps were used to microdissect the bag cell neuron clusters from the surrounding connective tissue. Using a fire-polished glass Pasteur pipette and gentle trituration, neurons were dissociated from the clusters and dispersed in tcASW onto 35 × 10 mm polystyrene tissue culture dishes (C353001; Falcon-Corning/Fisher Scientific; Ottawa, ON, Canada). Neurons were either plated as individual cells or paired manually. The latter was accomplished by moving fluid in and out of the pipette to push or pull a free neuron into contact with a neuron already adhered to the dish, typically resulting in soma-to-soma contact. Cultures were maintained in a 14°C incubator in tcASW and used within 2–3 days.

Whole Cell Voltage- and Current-Clamp Recordings from Cultured Bag Cell Neurons

Membrane potential or current was recorded from cultured bag cell neurons using EPC-8 amplifiers (HEKA Electronics/Harvard Apparatus; Saint-Laurent, QC, Canada) and the tight-seal, whole cell method (35) at room temperature (~22°C). Microelectrodes were pulled from 1.5-mm external/1.12-mm internal diameter, borosilicate glass capillaries (TW150F-4; World Precision Instruments; Sarasota, FL) and fire-polished to a resistance of 1–3 MΩ when filled with various intracellular salines (see third paragraph of this section). In pairs of cultured bag cell neurons, cells were designated as *neuron 1* and *neuron* 2, based on being recorded with the left and right amplifier, respectively. Our prior work showed that electrical coupling between these neurons was symmetrical, i.e., the same magnitude in both directions (29); as such, protocols were only run with *neuron 1* as presynaptic and *neuron 2* as postsynaptic. For single neurons, recordings were performed with either amplifier.

Pipette junction potentials were nulled immediately before seal formation; following a seal, the pipette capacitance (5–7 pF) was canceled. Upon membrane rupture, neuronal capacitance (300–900 pF) was also canceled, while the series resistance (3–5 MΩ) was compensated to 80% and monitored throughout the experiment. Input signals were low-pass filtered at 1 kHz (for current) and 5 kHz (for voltage) by the EPC-8 Bessel filter, and sampled at 2 kHz using a Windows-based personal computer, a Digidata 1322 A analog-to-digital converter (Molecular Devices; Sunnyvale, CA), and the Clampex acquisition program of pCLAMP v8.1 (Molecular Devices). Clampex was also used to control the membrane potential under voltage-clamp and inject current in current-clamp; in addition, neurons were manually set to −40 or −60 mV in current-clamp with constant bias current from the EPC-8 V-hold.

Most recordings were done with normal artificial seawater (nASW) (composition as per tcASW but with glucose and antibiotics omitted) in the bath and our standard K^+-aspartate-based intracellular saline in the pipette [composition in mM: 500 K^+-Asp, 70 KCl, 1.25 $MgCl_2$, 10 HEPES, 11 glucose, 10 glutathione, 5 ethylene glycol bis(aminoethyl ether) tetraacetic acid (EGTA), 5 adenosine 5′-triphosphate 2Na·H_2O (A3377; Sigma-Aldrich), and 0.1 guanosine 5′-triphosphate

Na·H_2O (G8877; Sigma-Aldrich); pH 7.3 with KOH]. Free Ca^{2+} was set at 300 nM by adding 3.75 mM $CaCl_2$, as calculated by WebMaxC (https://somapp.ucdmc.ucdavis.edu/pharmacology/bers/maxchelator/webmaxc/webmaxcS.htm), which corresponds to the approximate resting Ca^{2+} concentration in bag cell neurons (36–38). In some instances, K^+ current was isolated by using a Na^+-free/Ca^{2+}-free/high-Mg^{2+} artificial seawater (sfcfhmASW; composition in mM: 471 *N*-methyl-D-glucamine, 10.4 KCl, 66 $MgCl_2$, 15 HEPES; pH 7.8 with HCl) as the extracellular saline. The K^+-Asp-based intracellular saline had a calculated liquid junction potential of 15 and 23 mV versus nASW and sfcfhmASW, respectively. In a small number of experiments, 71.25 mM tetraethylammonium-Cl (TEA; AC150905000; Acros Organics; Morris Plains, NJ) was substituted equimolar for KCl in the intracellular saline, which resulted in a junction potential of 15 mV versus nASW. Last, Ca^{2+} current was isolated using a Ca^{2+}-Cs^+-TEA artificial seawater and intracellular saline where the K^+-Asp was replaced equimolar with Cs^+-Asp, which gave a junction potential of 20 mV. As mentioned, junction potentials were nulled before seal formation; thus, once whole cell mode was established, the holding potential was given by the command potential (from Clampex) minus the junction potential, which allowed for correction by off-line subtraction.

The time course and amplitude of voltage (for voltage-clamp) or current-injection (for current-clamp) protocols were set in Clampex; see RESULTS for details. Although junctional current and inward rectifier-like K^+ current were not leak-subtracted, a P/4 protocol was used to correct for a leak when measuring voltage-gated Ca^{2+} current and outward voltage-gated K^+ current. From a holding potential of −60 mV, four subpulses of opposite polarity and one-fourth the magnitude of the test pulse were delivered, with an intersubpulse interval of 500, and 100 ms before the actual test pulse. The leak current evoked by the subpulses was summed, inverted, and subtracted from the current elicited during the subsequent test step to reveal voltage-dependent current (38).

Recording Conditions, Drug Application, and Reagents

The culture dish served as the bath. Before the experiment, the tcASW was replaced with the desired extracellular saline using a calibrated transfer pipette to a final volume of 2 mL. On occasion, photomicrographs (1,392 × 1,040 pixels) of neurons were acquired using a Pixelfly USB camera (Photon Technology International, London, ON, Canada) and the Micro-Manager v1.4.5 plugin (http://micro-manager.org) for ImageJ v1.44n9 (http://rsbweb.nih.gov/ij/) with 100–200 ms exposures. In some experiments, phorbol-12-myristate-13-acetate (P8139; Sigma-Aldrich; stock in dimethyl sulfoxide) was added to the bath just before recording. Specifically, a small volume (~50 μL) of saline was initially removed from the bath, combined with an even smaller volume (<2 μL) of stock solution, then that mixture was reintroduced to the bath for a final concentration. Pressure ejection was used to apply acetylcholine (A6625; Sigma-Aldrich; dissolved in nASW at 2 mM) using a PMI-100 pressure ejector (Dagan; Minneapolis, MN) and 2-s, 75–100 KPa pulses via an unpolished whole cell pipette (1–2 μm tip diameter) positioned ~50 μm away from neuronal pairs. Aside from those reagents specified thus far, all other chemicals were from Acros Organics, Thermo Fisher Scientific, MP Biomedicals (Solon, OH), or Sigma-Aldrich.

Analysis

Most analyses involved pairs of bag cell neurons (*neuron 1* and *neuron 2*) with respective membrane potentials and membrane currents specified as V1, V2, I1, and I2; single neurons were examined in a similar fashion, but simply as V and I. The Clampfit (v8.1 or v10.2) analysis program of pCLAMP was used to determine the amplitude and time course of current or voltage, as well as the area above the curve and membrane potential synchrony. For changes in current, a pair of cursors, 5–20 ms apart, was placed 1 ms before the response evoked by a given voltage step, and the mean current between these two cursors was taken as baseline. If the change was measured at steady-state, another pair of cursors was placed during the response at 170 and 190 ms for a 200-ms step (see RESULTS for details) and the mean current was measured between these two cursors. That mean was compared with the baseline mean and taken as the steady-state amplitude. If the change was measured at the peak, a cursor was placed 1–5 ms after the onset of the response, while another cursor was placed well past the peak but before the end of the step. The peak change between these two cursors, relative to the preresponse baseline was then calculated as mentioned earlier.

For changes in voltage, a pair of cursors, also 5-20 ms apart, was placed 1 ms before the estimated inflection point of the response [hyperpolarization, electrotonic potential (ETP), action potential], and the mean voltage between these two cursors taken as baseline. For steady-state changes during a 1-s current step, another pair of cursors was placed at 898 and 998 ms of the response (see RESULTS for details), the mean voltage was measured between these cursors, and then compared with the baseline voltage. For peak changes, a cursor was placed 1–5 ms after the inflection point of the voltage change, while another cursor was placed after the peak. The peak change between these two cursors, relative to the baseline, was then calculated. Times of peak voltage change were determined by placing cursors before and after an action potential in *neuron 1* as well as the corresponding ETP in *neuron 2* and using a time-of-peak analysis function. The peak-to-peak latency between action potential and ETP was calculated as the difference between these times. ETP area was found by placing cursors at the inflection point of the response onset, as well as when the ETP initially returned to baseline, and taking the area between those cursors compared with the preresponse baseline. Firing synchrony was measured by comparing the time-shifted data between pairs of firing neurons using a cross-correlation analysis function with the number of lags at ±1,000.

Junctional or membrane current was plotted against test voltage using Prism v6.0–8.0 (GraphPad Software; La Jolla, CA), which was also used to make plots of coupling coefficient or input resistance versus current, as well as plots of the relative amplitude of the ETP, junctional current, or membrane current versus stimulus number (relative change obtained by dividing all responses by the first response; see RESULTS for details). Prism was also used to construct amplitude bar graphs and for linear regression analysis. The coupling coefficient was ascertained by the ratio of V2/V1, at the steady-state membrane potential during a hyperpolarizing current pulse to *neuron 1*. Input resistance was calculated in a similar way, except the steady-state voltage response of a

neuron was divided by the amount of current injected into that same neuron.

Statistics were performed using InStat v3.1 (GraphPad Software). Data are presented as the means ± standard deviation with individual data points shown when feasible. The Kolmogorov–Smirnov method was used to test data sets for normality. For normally distributed data, Student's paired or unpaired *t* test was used to test for differences between two means, while an ordinary one-way analysis of variance (ANOVA) or repeated-measures one-way ANOVA, with the Dunnett's multiple comparisons posttest, was used to test for differences between multiple means. In one case, Bonferroni-corrected paired Student's *t* tests were used to test between multiple means (see RESULTS for details). For not-normally distributed data, an unpaired Mann–Whitney *U* test or Wilcoxon matched-pairs test was used to compare two groups, whereas a Kruskal–Wallis one-way ANOVA (KW-ANOVA) with Dunn's multiple comparisons test was used to compare between multiple groups. An *F* test was used to determine if the slope provided by linear regression was different from a slope of zero. A difference was considered statistically significant if the two-tailed *P* value was < 0.05; the only exception to this was a Bonferroni-corrected *P* value of < 0.001 (see RESULTS for details). Whenever possible, in accordance with the output of the software, exact *P* values are reported.

RESULTS

Bag Cell Neurons Form Electrical Synapses in Culture

The extensive electrical coupling between bag cell neurons in the intact cluster restricts how electrical transmission can be studied ex vivo (25, 29, 30). Hence, as we have done previously (29, 39, 40), bag cell neurons were paired in culture to form electrical synapses (see METHODS, *Animals and Cell Culture* for details). Most pairs were plated with somata making contact (Fig. 1*A*), which was preferred because it provided a stronger connection than axon-axon contact (41). The electrical transmission was detectable between neurons under whole cell current-clamp using Na^+-based normal artificial seawater (nASW) as extracellular saline and K^+-Asp-based intracellular saline in the pipettes (see METHODS, *Whole Cell Voltage- and Current-Clamp Recordings from Cultured Bag Cell Neurons* for details). Neurons were designated as *neuron 1* for presynaptic and *neuron 2* for postsynaptic. With both cells at the typical bag cell neuron resting potential of −60 mV (27, 42–44), an action potential evoked in *neuron 1* consistently produced an electrotonic potential (ETP) in *neuron 2* ($n = 20$ pairs) (Fig. 1*B*). The average peak amplitude of the ETP was ∼11 mV (Fig. 1*B*, *lower inset*).

Akin to our earlier reports (29, 39, 40), coupled bag cell neurons also presented junctional current under whole cell voltage-clamp. At a holding potential of −60 mV for both cells, a protocol of square pulses from −90 mV through to +60 mV was given to *neuron 1*, while maintaining *neuron 2* at −60 mV (Fig. 1*C*, *upper* and *lower middle*). The presynaptic steps elicited a mix of voltage-dependent membrane currents from *neuron 1* and junctional currents from *neuron 2* (Fig. 1*C*, *upper middle* and *lower*). The postsynaptic (junctional) current reflected what was needed to keep *neuron 2* clamped at −60 mV when a presynaptic pulse created a voltage difference across the gap junction. During steps up to −10 or 0 mV, the junctional current showed little inactivation, but at pulses >0 mV, partial inactivation was apparent ($n = 29$–42 pairs; *n* values are not uniform because steps >0 mV were not always delivered to *neuron 1*, and in some cases, voltages ≥ +40 mV evoked outward current in *neuron 1* that exceeded the amplifier output). The current/voltage relationship of the mean steady-state junctional current in *neuron 2* versus the presynaptic voltage step in *neuron 1* was linear between −90 and 0 mV, whereas modest rectification was evident between 0 and +60 mV (Fig. 1*D*). On average, during the −90 mV step, the steady-state junctional current was outward at ∼+200 pA, whereas during the +60 mV step, it was inward at ∼−400 pA.

Input Resistance, but Not Coupling Coefficient, Declines with Increasing Hyperpolarization

Prior examination of the coupling coefficient between pairs of bag cell neurons was based on the postsynaptic response to a solitary and/or brief presynaptic hyperpolarization (29, 45). To determine if presynaptic voltage influences electrical transmission, we tested the coupling coefficient over a range of more lengthy negative current injections. With both cells initially current-clamped at −60 mV, hyperpolarization of *neuron 1*, with pulses from −50 to −250 pA, was transferred to *neuron 2* ($n = 28$ pairs) (Fig. 2*A*). The mean *neuron 1* to *neuron 2* coupling coefficient, measured at steady-state voltages, was a constant ∼0.55 and showed no significant difference across all current injection magnitudes (Fig. 2*B*). Accordingly, linear regression of this relationship yielded a line with a slope ($m = 0.000075$) that was not significantly different from zero, indicating coupling coefficient was voltage-independent. There was also an attenuation in the voltage response of *neuron 1* during current injection, in that the hyperpolarization did not grow proportionately with greater current (Fig. 2*A*, *middle*). This anomalous rectification was noticeable in the relationship between *neuron 1* input resistance and current injection magnitude, i.e., the greater the hyperpolarization, the smaller the average *neuron 1* input resistance, again taken at steady-state (Fig. 2*C*). Linear regression furnished a line with a slope ($m = 0.39$) that was significantly different from zero.

Presynaptic Action Potential-Like Waveforms from the Slow-Phase of the Afterdischarge Evoke Facilitating Postsynaptic ETPs in a Use-Dependent Manner

We next considered how both action potential dynamics and repeated presynaptic firing influences electrical transmission. As the fast then slow phases of the afterdischarge proceed, the height and width of the action potential change, along with spike frequency (23, 46) (see INTRODUCTION for details). Instead of simply using current injection to elicit firing, the presynaptic spike was standardized by delivering fast- or slow-phase action potential-like waveforms to *neuron* 1 under voltage-clamp, while measuring the postsynaptic response in *neuron 2* under current-clamp. Similar to our previous work (40), these waveforms were derived from spikes recorded in bag cell neurons during bona fide afterdischarges in intact clusters (24, 29, 47). Both waveforms started at a holding potential of −40 mV, followed by a 25-ms ramp to +30 mV (for fast-phase) or +40 mV (for slow

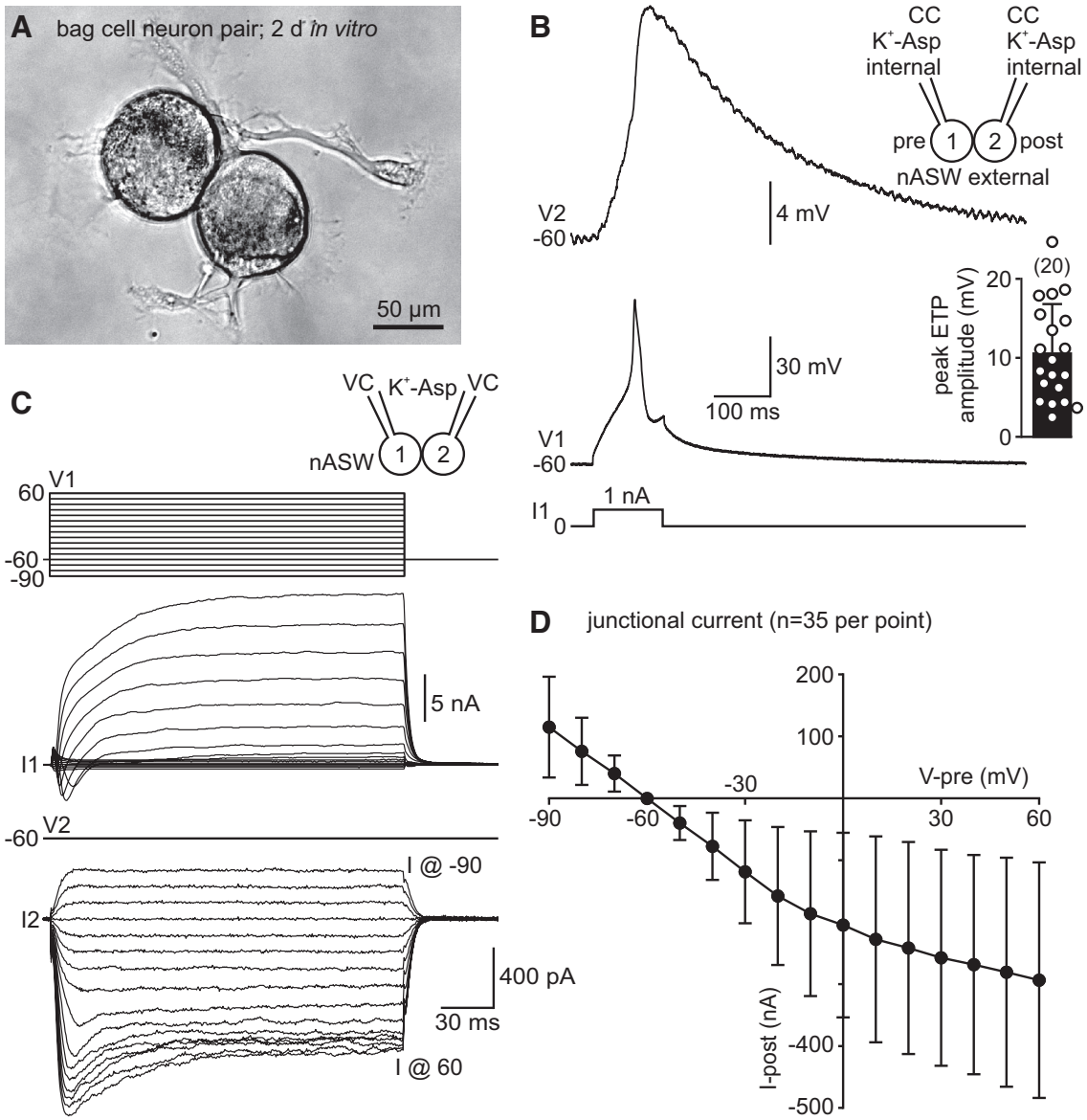

Figure 1. Cultured bag cell neurons are electrically coupled and present a largely linear junctional current/voltage relationship. *A*: a pair of bag cell neurons after 2 days in primary culture. Contact is made both at the somata and between overlapping neurites, particularly in the upper portion of the photomicrograph. *B*: dual recording from paired bag cell neurons in vitro. *Upper inset*: neurons are bathed in normal artificial seawater (nASW) and whole cell current-clamped (CC) using K^+-Asp based intracellular saline. With neurons set to −60 mV via bias current, a presynaptic (pre) action potential in *neuron 1* (V1; *middle*) evoked by a 100-ms, 1-nA current pulse (I1; *lower*) elicits a postsynaptic (post) electrotonic potential (ETP) in *neuron 2* (V2; *upper*). The onset of depolarization in *neuron 2* precedes the spike in *neuron 1*. *Lower inset*: summary of mean peak amplitude of the ETP; number above bar is *n*-value that reflects number of pairs. Abscissa applies to both traces. *C*: dual whole cell voltage-clamp of an electrically coupled pair; different neurons from *B*. *Inset*: conditions as per *A*, but under voltage-clamp (VC). Both neurons are held at −60 mV, then *neuron 1* is stepped from −90 to +60 mV in 200-ms, 10-mV increments (V1; *upper*) while *neuron 2* is kept at −60 mV (V2; *lower middle*). This evokes voltage-dependent membrane current in *neuron 1* (I1; *upper middle*) and junctional current in *neuron 2* (I2; *lower*). For *neuron 1*, inward current is apparent near the start of the step, starting at −10 mV, and is likely Ca^{2+}; this is then overwhelmed by delayed outward K^+ current. For *neuron 2*, junctional current is outward with presynaptic steps negative to −60 mV, and inward with steps positive to −60 mV. Junctional current does not inactivate during steps up to 0 mV, but undergoes some inactivation at more positive voltages. Abscissa applies to both traces. *D*: plot of mean steady-state postsynaptic current from *neuron 2* (I-post), i.e., junctional current, vs. the presynaptic voltage (V-pre) step reveals a linear, voltage-independent association from −90 to 0 mV, and modest rectification from 0 to +60 mV. *n* value indicates number of pairs.

phase), then a 20-ms ramp to +5 mV (for fast phase) or a 40-ms ramp to +15 mV (for slow phase), and two subsequent ramps of 25 ms to −50 mV and 50 ms to −40 mV (for both phases) (Fig. 3*A*, *lower left* and *right*). Before stimulation, *neuron 2* was current-clamped to −40 mV, which corresponds to the common interspike membrane potential during an afterdischarge (24, 27).

Pairs of coupled bag cell neurons were recorded in nASW using K^+-Asp-based intracellular saline. Giving either the fast- (n = 9 pairs) or slow-phase (n = 8 pairs) action potential-like waveform to a voltage-clamped *neuron 1*, triggered an ETP in a current-clamped *neuron 2* (Fig. 3*A*, *upper left* and *right*). Although the peak amplitude of the ETP induced by the slow-phase waveform trended higher, it

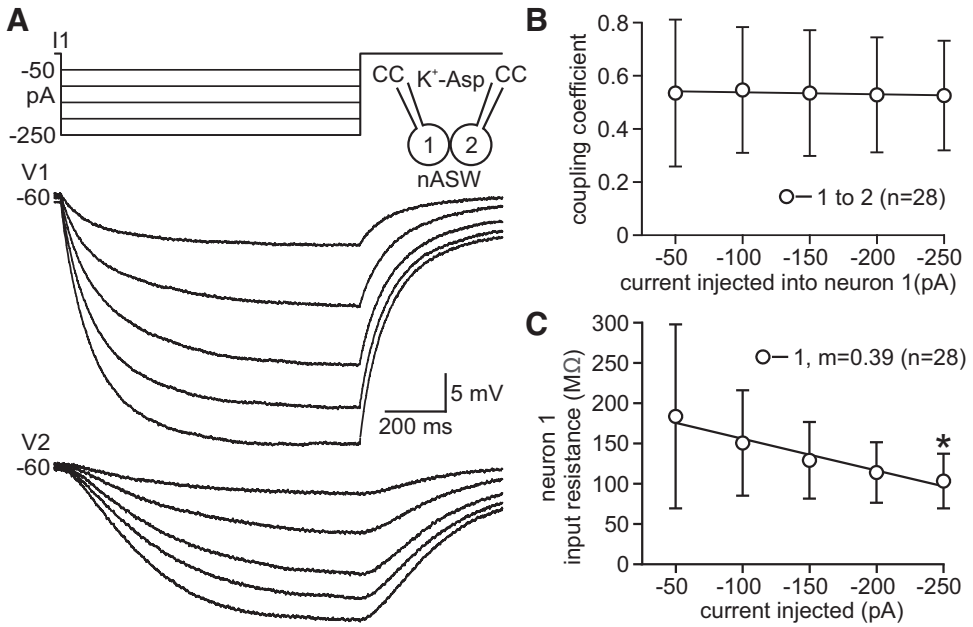

Figure 2. With increasing hyperpolarization, input resistance falls while coupling coefficient remains constant. *A*: electrically coupled bag cell neurons in normal artificial seawater (nASW) are current-clamped (CC) to −60 mV with bias current using K^+-Asp-based intracellular saline (*inset*). Injecting *neuron 1* with 1-s pulses of −50 to −250 pA in 50-pA increments (I1; *upper*) hyperpolarizes *neurons 1* (V1; *middle*) and *2* (V2; *lower*). Anomalous rectification, i.e., voltage attenuation, is apparent with −200 and −250 pA. Scale bars apply to both traces. *B*: summary plot showing the average *neuron 1* to *neuron 2* coupling coefficient remains unchanged regardless of the current magnitude injected into *neuron 1* ($F_{14,135}$ = 0.03386, P = 0.9978, ordinary one-way ANOVA; m = 0.000075, R^2= 0.5234, linear regression fit; $F_{1,3}$ = 3.295, P = 0.1671, F test, not significantly different from slope of zero). n value indicates number of pairs. *C*: mean *neuron 1* input resistance decreases with greater hyperpolarization (H = 17.719, dF = 4, P = 0.0014, KW-ANOVA; *$P < 0.01$ −50 vs. −250, not significant −50 vs. −100, −150, and −200, Dunn's multiple comparisons test). Straight line represents linear regression fit (m = 0.39, R^2= 0.9538; $F_{1,3}$ = 61.95, P = 0.043, F-test, significantly different from slope of zero). n value indicates number of neurons.

was not significantly different from the response elicited by the fast-phase waveform (Fig. 3*B*). However, the mean ETP area and mean peak-to-peak presynaptic waveform-to-ETP latency were both significantly larger for slow-phase stimulation (Fig. 3, *C* and *D*).

Because the afterdischarge firing frequency varies from ~5 Hz in the fast phase to ~1 Hz in the slow phase (see INTRODUCTION for details), we also examined the response to 10-s trains of stimulation. Again, *neuron 1* was voltage-clamped at a holding potential of −40 mV and *neuron 2* current-clamped to −40 mV. The fast-phase waveform (Fig. 4*A*, *upper right*) was delivered at 5 Hz for 10 s (50 stimuli), and resulted in ETPs that did not vary appreciably in amplitude during the train stimulus (n = 23 pairs) (Fig. 4*A*, *upper left and middle*). Nevertheless, applying the slow-phase waveform (Fig. 4*A*, *lower right*) at 1 Hz for 10 s (10 stimuli), provoked ETPs that grew in a use-dependent fashion as the train stimulus progressed (n = 30 pairs) (Fig. 4*A*, *lower left and middle*). During the fast-phase train stimulus, the average normalized change in the peak of the ETP was an ~5% increase from the initial, but this did not reach significance, except for the responses to the 31st and 50th waveforms (Fig. 4*B*). Given that there are 49 pairings in this comparison, the significant difference seen at these two, specific ETPs may well be due to chance. In keeping with that possibility, a secondary statistical analysis comparing the first ETP to each subsequent ETP using Bonferroni-corrected multiple paired Student's t tests found no significant difference (significance level Bonferroni corrected to $P < 0.001$, i.e., $P < 0.05/49$). Conversely, during the slow-phase train stimulus, the average normalized peak ETP facilitated soon after the start of the protocol, and then plateaued at a 10–15% increase, with the ETPs evoked by waveforms 3 through 10 being significantly greater than the first ETP (Fig. 4*C*).

Facilitation of the ETP Reflects a Use-Dependent Change in Postsynaptic Responsiveness Rather than Junctional Current

Given that the fast-phase action potential-like waveform train stimulus did not alter the ETP to any great extent, we focused on addressing the mechanism of use-dependent facilitation brought about by the slow-phase train stimulus. The latter could increase the ETP by enhancing the junctional current and/or augmenting how the postsynaptic membrane reacts to presynaptic input. A possible change to junctional current was tested in coupled pairs of bag cell neurons under dual voltage-clamp with K^+-Asp-based intracellular saline and nASW extracellular saline. From a holding potential of −40 mV for both neurons, the 1-Hz, 10-s slow-phase train stimulus was delivered to *neuron 1* (10 stimuli) while maintaining *neuron 2* at −40 mV (Fig. 5*A*, *lower*). This induced an ~−300 pA inward junctional current in *neuron 2* (Fig. 5*A*, *inset*), which was roughly triangular in shape with an accelerated onset and slower to return to baseline (n = 20 pairs) (Fig. 5*A*, *upper*). Still, the size and dynamics of the junctional current remained constant throughout the train stimulus (Fig. 5*B*). On average, the normalized peak junctional current showed no significant change over the 10 s (Fig. 5*C*).

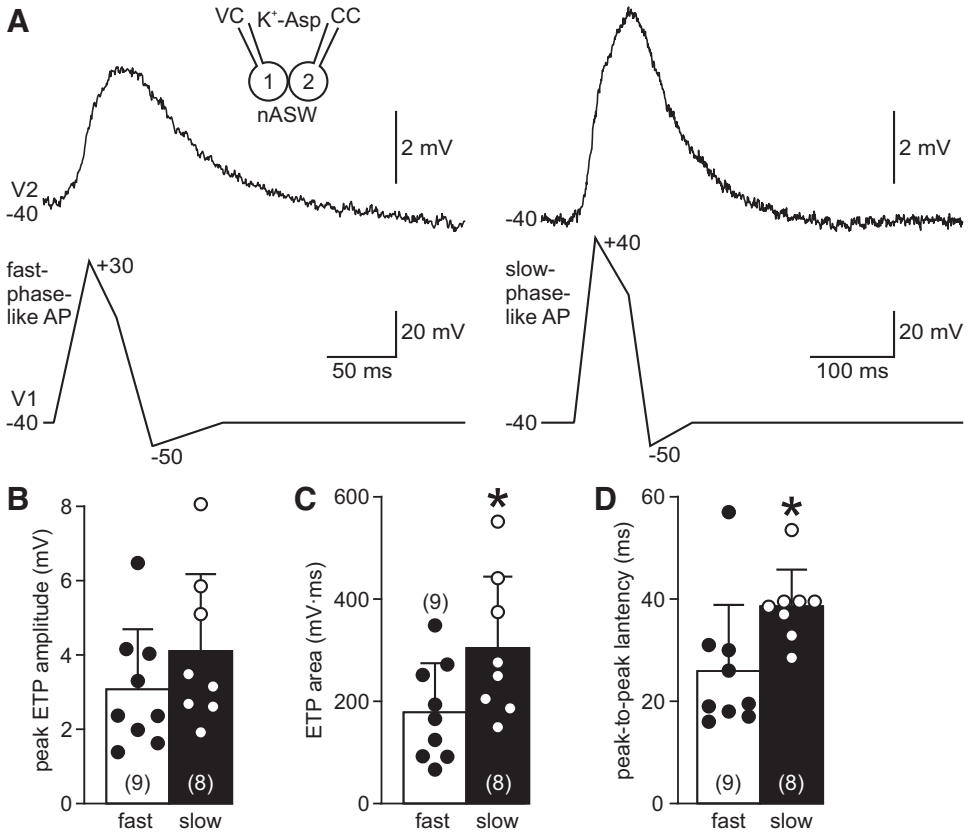

Figure 3. Presynaptic fast- and slow-phase action potential-like waveforms elicit postsynaptic ETPs. *A*: in a pair of electrically coupled bag cell neurons, *neuron 1* is voltage-clamped (VC) at −40 mV while *neuron 2* is current-clamped (CC) to −40 mV with bias current using K^+-Asp-based intracellular saline and normal artificial seawater (nASW) external saline (*inset*). Voltage-clamp waveforms, mimicking the action potential (AP) from the fast- (V1; *lower left*) or slow-phase (V1; *lower right*) of the afterdischarge, delivered to *neuron 1* evokes an electrotonic potential (ETP) in *neuron 2* (V2; *upper*); waveforms are described in detail in RESULTS text. Depolarizations in *neuron 2* occur almost concurrently with the initial ramp of the waveforms in *neuron 1*. *Left* abscissa applies to *upper* and *lower left* traces; *right* abscissa applies to *upper* and *lower right* traces. *B*: the mean peak ETP amplitude is not different between the fast- and slow-phase action potential waveform stimulus (t_{15}= 1.150, P = 0.2682, unpaired Student's t test). For *B* as well as *C* and *D*, numbers in bars are n values that indicate number of pairs. *C*: however, the average ETP area produced by the slow-phase waveform is significantly larger (t_{15}=2.116, *P = 0.0468, unpaired Student's t test). *D*: similarly, the mean latency of the peak of the stimulus waveform to the peak of the ETP is also significantly longer for the slow-phase condition ($U_{8,9}$ = 10.000, *P = 0.0139, Mann–Whitney U test).

To determine whether the postsynaptic neuron itself was adapting as the train stimulus progressed, a protocol was designed based on the junctional current induced by the slow-phase action potential-like waveform. Modeled after the outcomes in Fig. 5, this depolarizing current consisted of a 27-ms ramp from 0 to +300 pA, followed by a 68-ms ramp back down to 0 pA (Fig. 6*A*, *lower*). The junctional-like current waveform was injected as a 1-Hz, 10-s train stimulus into individual bag cell neurons current-clamped at −40 mV (10 stimuli). This evoked depolarizations that were kinetically similar to synaptic ETPs; moreover, this "ETP" facilitated in a use-dependent manner over the course of the train stimulus (n = 39 cells) (Fig. 6*A*, *upper* and Fig. 6*B*). Compared with initial, the mean normalized peak "ETP" was significantly larger starting at the 5th current injection and finished ∼10% bigger by the end of the protocol (Fig. 6*C*).

Voltage-Gated Ca^{2+} Current Decreases Minimally during a Train Stimulus of ETP-like Waveforms

The depolarization of the ETP may be sufficient to activate voltage-gated currents, which in turn could undergo use-dependent alterations and change postsynaptic responsiveness. Two possible candidates are the Ca^{2+} current and certain K^+ currents; bag cell neurons have limited-to-no expression of voltage-gated Na^+ current (43, 48), so were not investigated here. We already showed that modest depolarizations can activate Ca^{2+} current (40, 49), although its behavior during repetitive ETP-like stimulation is unknown. Ca^{2+} current from individual bag cell neurons was recorded under voltage-clamp with Cs^+-Asp-based intracellular saline and Ca^{2+}-Cs^+-TEA ASW extracellular saline as per our prior efforts (see METHODS, *Whole Cell Voltage- and Current-Clamp Recordings from Cultured Bag Cell Neurons* for details) (50). From a −60 mV holding potential, 10-mV incremental steps to +40 mV elicited rapidly activating and moderately inactivating voltage-dependent inward current (n = 22 cells) (Fig. 7*A*). The grouped data of the peak current/voltage relationship was stereotypically U-shaped (Fig. 7*B*), similar to what we and others have reported (46, 48, 50, 51).

For the Ca^{2+} current to contribute to the use-dependent facilitation of the ETP, it would have to increase with repetitive depolarization, so as to provide greater drive during each subsequent ETP. To ascertain if this was the case, the postsynaptic voltage change was standardized by applying waveforms derived from the "ETP" response of neurons injected with junctional-like current, as presented in Fig. 6. The ETP-like waveform began from a −40 mV holding potential, followed by a 68-ms ramp to −19 mV, held at −19 mV for 15 ms, then a 45-ms ramp to −30 mV, and a 58-ms ramp back to −40 mV (Fig. 7*C*, *upper*). This slow-phase ETP-like waveform train stimulus was given under a voltage-clamp for 10 s at 1 Hz (10 stimuli), and provoked Ca^{2+} current that decreased sparingly in a use-dependent manner (n = 7 cells) (Fig. 7*C*, *lower*). When normalized and averaged, the peak Ca^{2+} current was significantly smaller at waveforms 8 through 10, although this drop was only by 2–3% compared with the start (Fig. 7*D*).

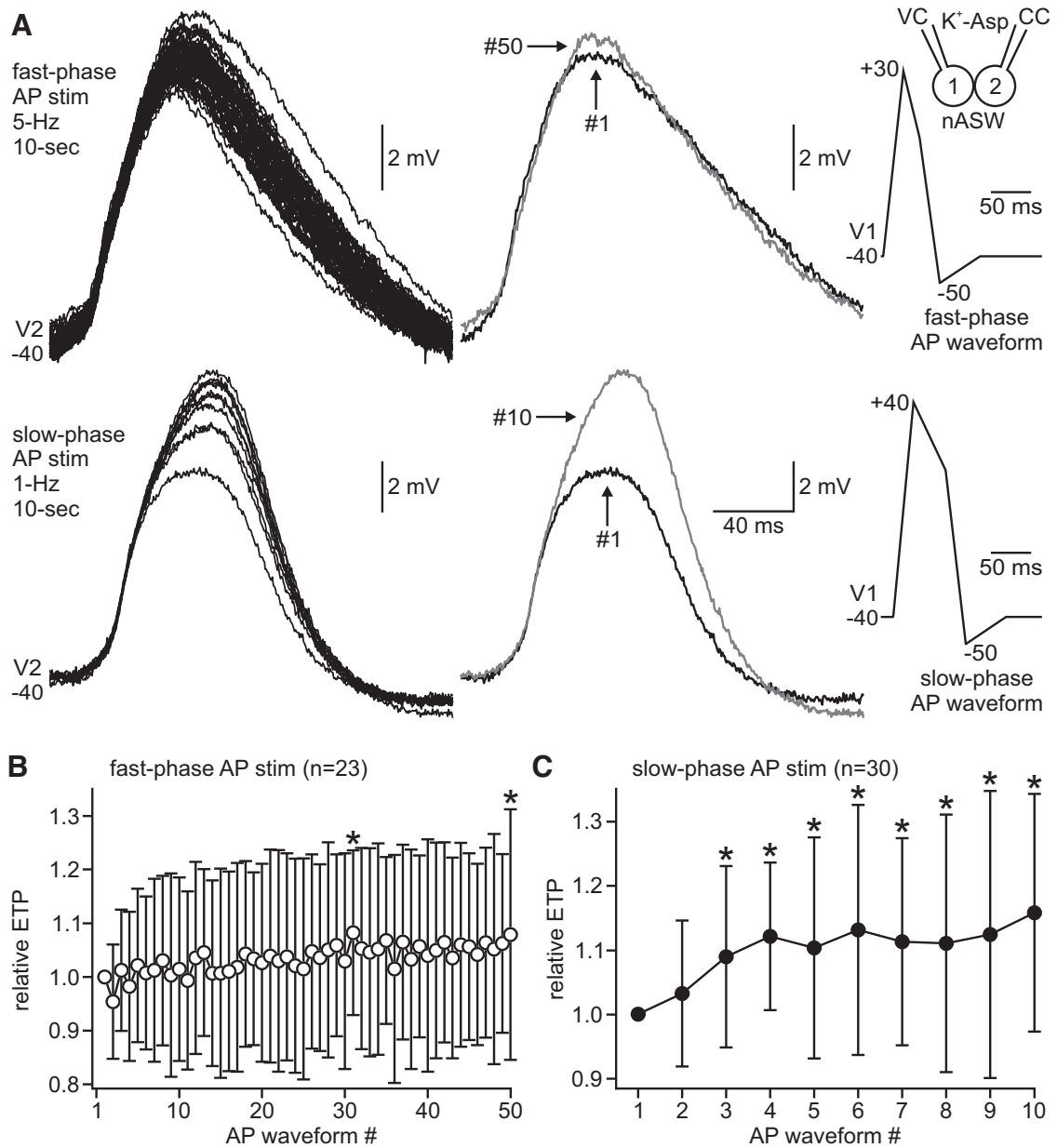

Figure 4. Repetitive presynaptic stimulation at 1 Hz, but not 5 Hz, evokes facilitating ETPs. *A*: a coupled bag cell neuron pair is bathed in normal artificial seawater (nASW) and whole cell recordings made using K^+-Asp-based intracellular saline (*inset*). While voltage-clamping (VC) *neuron 1* at −40 mV and current-clamping (CC) *neuron 2* to −40 mV with bias current, a 10-s train stimulus (stim) of fast- (5 Hz; V1; *upper right*) or slow-phase (1 Hz; V1; *lower right*) action potential (AP)-like waveforms (in mV) given to *neuron 1* results in an electrotonic potential (ETP) in *neuron 2* (V2). *Upper* and *lower left* show all ETPs overlaid (50 for fast-phase and 10 for slow-phase); for clarity, *upper* and *lower middle* display the first (black) and last (gray) trace. While the ETP changes little during the 5-Hz train stimulus, the response steadily increases through the 1-Hz train stimulus. Numbers refer to the 1st, 10th, or 50th ETP. Abscissa applies to all *middle* and *right* traces. *B*: group data of relative peak ETP amplitude, obtained by dividing all ETPs by the first ETP in a given pair, during the fast-phase train stimulus. The response trends up, but only the ETP following the 31st and 50th waveforms are significantly greater than the 1st ($F_{49,1078}$ = 1.826, P = 0.0006, repeated-measures one-way ANOVA; *$P < 0.05$, Dunnett multiple comparisons test). *n* value indicates number of pairs. *C*: the relative change in the average peak ETP during the slow-phase train stimulus is an initial increase and then levelling off, with a significant difference in the response induced by the 3rd to the 10th waveform compared with the 1st ($F_{9,261}$ = 7.125, $P < 0.0001$, repeated-measures one-way ANOVA; *$P < 0.01$, Dunnett multiple comparisons test). *n* value indicates number of pairs.

Voltage-Gated K^+ Current Cumulatively Inactivates during a Train-Stimulus of ETP-Like Waveforms

Having ruled out Ca^{2+} current, we next looked at whether there was any run-down of the voltage-gated K^+ current during the ETP-like train stimulus. The rationale was that a cumulative inactivation of outward current could enhance postsynaptic responsiveness and mediate use-dependent facilitation of the ETP. The major K^+ currents in bag cell neurons are a transient I_A current and two delayed rectifier I_K currents (48). At membrane potentials $\leq$−60 mV, I_A is inactivated (52), but the I_K are available for recruitment (53), making the latter viable prospects. Using K^+-Asp-based intracellular saline and a sfcfhmASW extracellular saline to

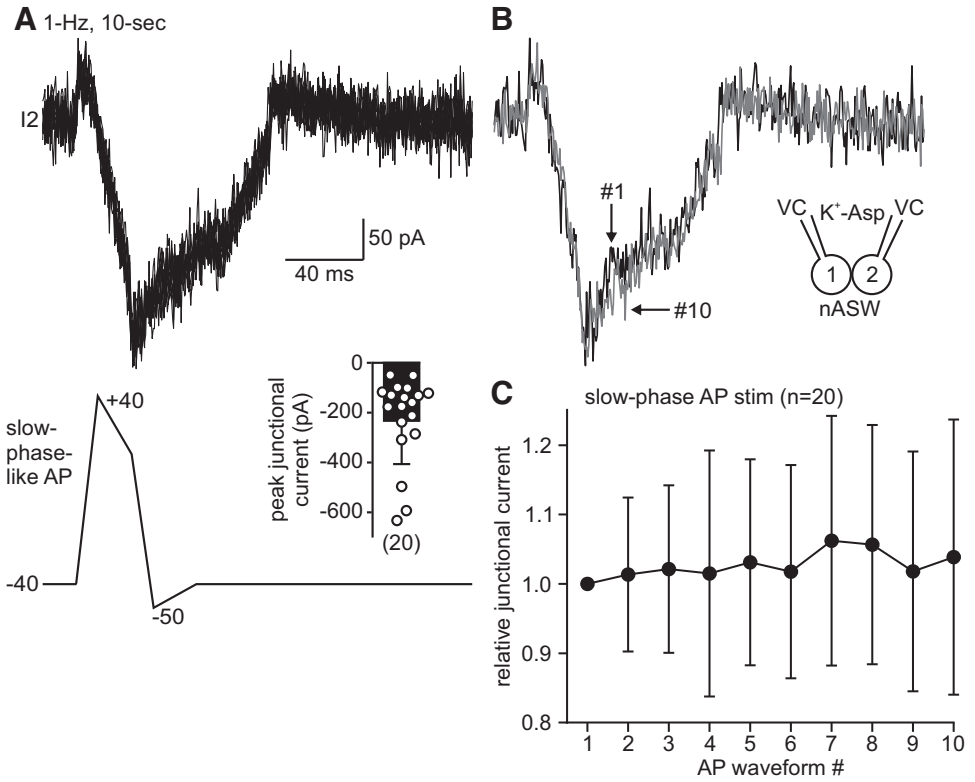

Figure 5. Junctional current is unchanged during repetitive presynaptic slow-phase action-potential-like stimulation. *A*: a coupled pair of bag cell neurons is voltage-clamped (VC) in normal artificial seawater (nASW) with K^+-Asp-based intracellular saline. *Lower*: both neurons are held at −40 mV and a 1-Hz, 10-s train stimulus (stim) of slow-phase action potential (AP)-like waveforms is applied to *neuron 1* (V1). *Upper*: the 10 resulting junctional currents in *neuron 2* (I2) are overlaid and show a characteristic, rapid inward component followed by a slower recovery, but change little during the train stimulus. *Inset*: summary data for peak amplitude of the first junctional current; number above bar is *n* value that reflects number of pairs. Scale bars apply to both *A* and *B*. *B*: junctional currents at 1 s (black) and 10 s (gray) are displayed for clarity. *Inset*: recording conditions. *C*: *left*, mean plot of the relative peak junctional current during the slow-phase train stimulus. There is no significant change in the currents evoked by waveform 2 through 10 compared with 1 ($F_{9,171} = 0.9289$, $P = 0.5015$, repeated-measures one-way ANOVA). *n* value indicates number of pairs.

isolate K^+ current, individual bag cell neurons were whole cell voltage-clamped at −60 mV. Pulsing the neuron to +40 mV in 10-mV increments induced outward K^+ current with a less rapid onset compared with the Ca^{2+} current, as well as some inactivation at test potentials >+10 mV (*n* = 33–36 cells; *n* values are not uniform because in some cases current evoked at +30 or +40 mV exceeded the amplifier output) (Fig. 8*A*). The steady-state current/voltage relationship of the grouped data showed an onset between −40 and −30 mV with outward rectification (Fig. 8*B*), comparable with data published by ourselves and others (53, 54). The K^+ current was then examined during the 1-Hz, 10-s slow-phase

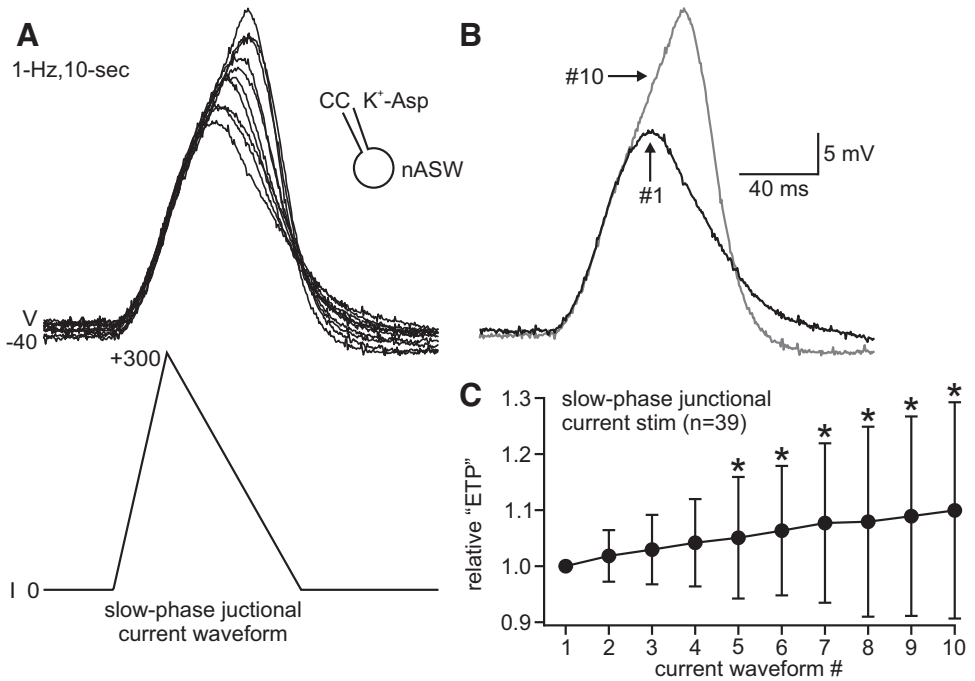

Figure 6. Repetitive slow-phase junctional-like current stimulation evokes a use-dependent facilitating "ETP". *A*: current-clamp recording from a single bag cell neuron with K^+-Asp-based intracellular saline and normal artificial seawater (nASW) external saline (*inset*). *Lower*: a 1-Hz, 10-s train stimulus of 300-pA depolarizing junctional-like current is applied (I; see RESULTS for details of current waveform) to a neuron set at −40 mV with bias current. *Upper*: the elicited voltage responses (V), which resemble a synaptic electrotonic potential (ETP), are overlaid. These ETPs increase in size with each subsequent current stimulus. *B*: just the response at 1 s (black) and 10 s (gray) are displayed for clarity. Scale bars apply to both *A* and *B*. *C*: summary plot demonstrates how the peak of the relative ETP becomes steadily larger over the course of the slow-phase junctional-like current train stimulus, and this difference is significant for the response to the 5th through 10th current waveform compared with the 1st ($F_{9,342} = 7.790$, $P < 0.0001$, repeated-measures one-way ANOVA; *$P <$ 0.05 for 5 s, *$P <$ 0.01 for 6–10 s, Dunnett multiple comparisons test). *n* value indicates number of single neurons.

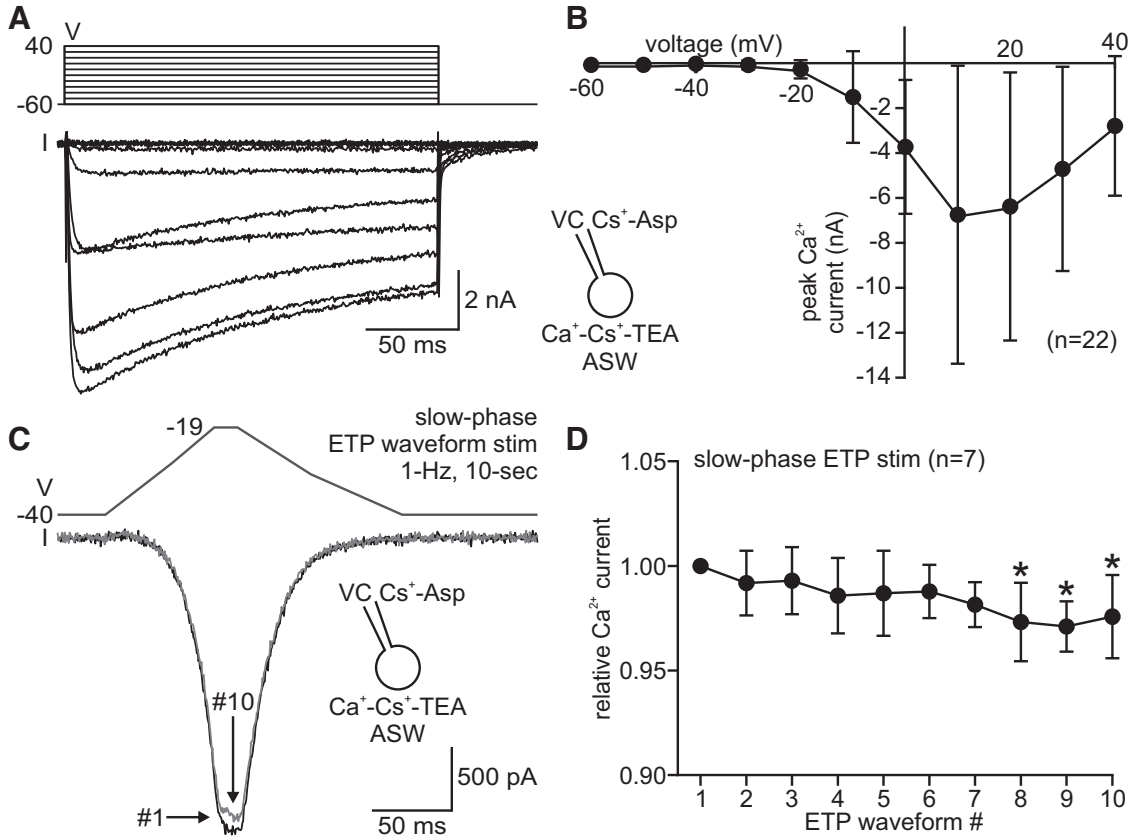

Figure 7. Repetitive slow-phase ETP-like stimulation does not facilitate Ca^{2+} current. *A*: a single bag cell neuron is voltage-clamped (VC) in Ca^{2+}-Cs^{+}-tetraethylammonium (TEA) artificial seawater (ASW) using Cs^{+}-Asp-based intracellular saline to isolate Ca^{2+} current (*inset*). From a holding potential of −60 mV, 200-ms pulses to +40 mV in 10-mV increments (V; *upper*) evoke voltage-dependent Ca^{2+} currents (I; *lower*). *B:* plot of average peak Ca^{2+} current against step voltage shows an onset between −30 and −20 mV. The largest current is at +10 mV but decreases above that as the conductance approaches reversal potential. *n* value indicates number of single neurons. *C*: under the same conditions as *A*, a waveform (in mV) mimicking the electotonic potential (ETP) elicited by slow-phase junctional current stimulation is delivered to a neuron voltage-clamped at −40 mV (V; *upper*); waveform is described in detail in the RESULTS. A 1-Hz, 10-s train stimulus (stim) of the waveform produces a modest Ca^{2+} current that changes little over time (I; *lower*). For clarity, only the response at 1 s (black) and 10 s (gray) are shown. *D*: mean data of the relative peak Ca^{2+} current during the slow-phase ETP waveform train stimulus. The current trends down to a small degree, with a significant difference in the current induced by the 8th through 10th waveform compared with the 1st ($F_{9,54} = 3.852$, $P = 0.0008$, repeated-measures one-way ANOVA; $*P < 0.01$, Dunnett multiple comparisons test). *n* value indicates number of single neurons.

ETP-like waveform train stimulus, again from a holding of −40 mV (Fig. 8*C*, *upper*). The protocol (10 stimuli) elicited a K^{+} current that progressively ran down (n = 19 cells) (Fig. 8*C*, *lower*). The mean normalized peak K^{+} current dropped immediately by ~3% and continued to fall until plateauing at an ~8% decrease, with the current provoked by waveforms 2 through 10 being significantly smaller versus that by waveform 1 (Fig. 8*D*).

Cumulative inactivation fits with the hypothesis that a loss of K^{+} current may boost responsiveness and in turn the amplitude of successive ETPs. As such, we sought to manipulate the current during electrical transmission using the classical K^{+} channel blocker, TEA (55, 56). Our previous work showed that TEA does not pass through bag cell neuron gap junctions when introduced intracellularly to just one of the two paired neurons, although it readily blocks K^{+} current from the inside (29). Hence, to try and prevent the facilitation of the ETP by occluding K^{+} current in the postsynaptic cell, TEA was added to the intracellular solution of the *neuron 2* recording pipette. The concentration of TEA was first established by monitoring K^{+} current in individual neurons with either 570, 285, 142.5, or 71.25 mM intracellular TEA, i.e., full, half, one-quarter, or one-eighth equimolar replacement of K^{+} with TEA. The 71.25 mM concentration reduced the K^{+} current by ~50% (n = 7 cells), whereas all higher concentrations blocked the current almost entirely, and anything lower had too variable of an effect to be useful (data not shown).

Electrically coupled pairs were then bathed in nASW and *neuron 1* was held at −40 mV under voltage-clamp with regular K^{+}-Asp-based intracellular saline (500 mM K^{+}-Asp and 70 mM KCl), while *neuron 2* was initially set to −40 mV under current-clamp with intracellular saline containing 498.75 mM K^{+}-Asp and 71.25 mM TEA-Cl. When the 1-Hz, 10-s train stimulus of slow-phase action potential-like waveforms was given to *neuron 1* (10 stimuli) (Fig. 8*E*, *upper*), it predictably evoked ETPs in *neuron 2* (n = 4) (Fig. 8*E*, *lower*). Furthermore, occluding run-down by preemptively inhibiting postsynaptic K^{+} current with TEA, resulted in the ETP remaining unaltered. The average relative peak ETP did not change significantly as the protocol went forward (Fig. 8*F*).

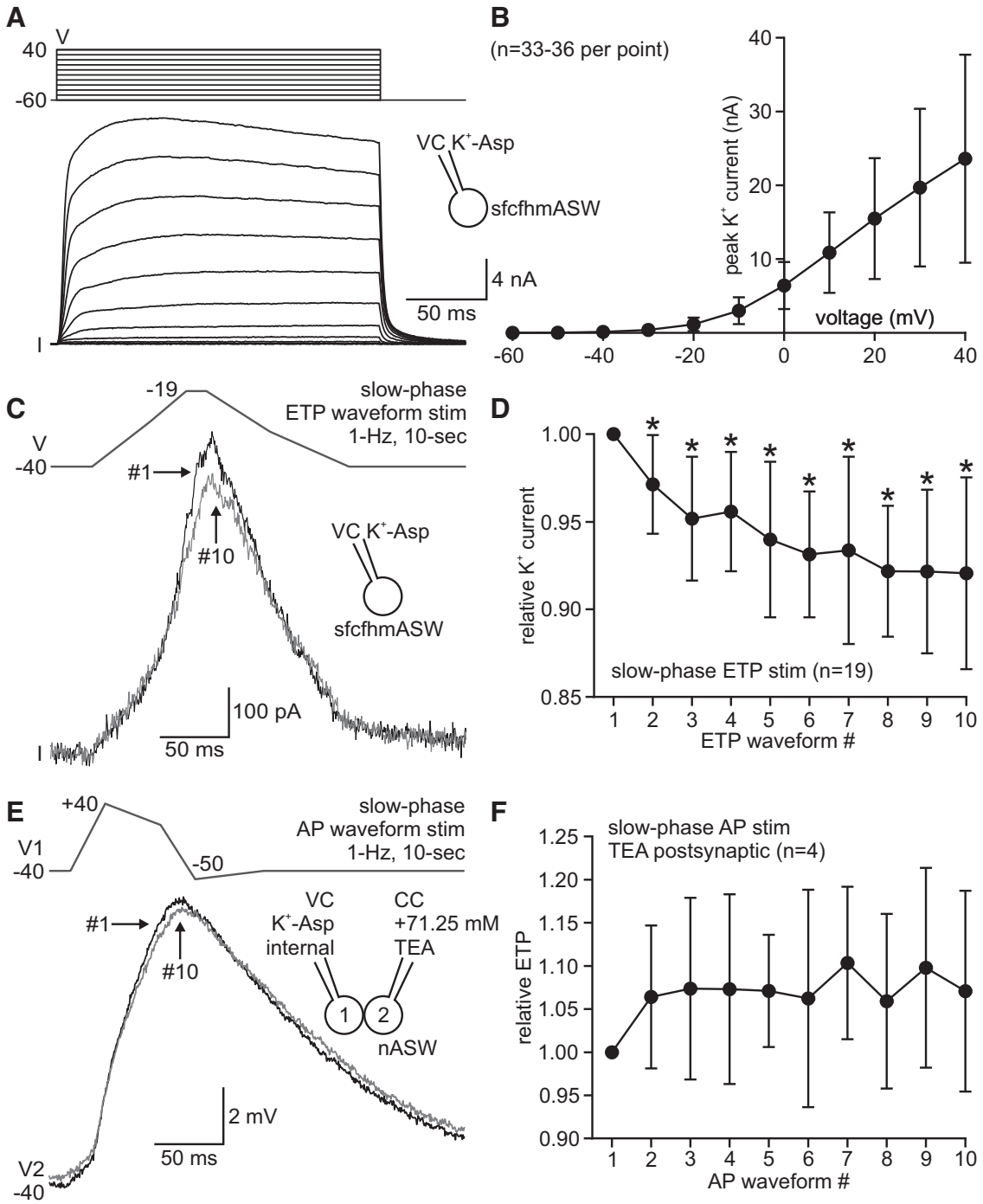

Figure 8. Repetitive slow-phase electotonic potential (ETP)-like stimulation causes cumulative inactivation of K^+ current. *A*: voltage-clamp (VC) recording from a single bag cell neuron in a Na^+-free/Ca^{2+}-free/high-Mg^{2+} artificial seawater (sfcfhmASW) using K^+-Asp-based intracellular saline to isolate K^+ current (*inset*). A series of 200-ms steps to + 40 mV) in 10-mV increments is delivered from a holding potential of –60 mV (V; *upper*), which elicits largely noninactivating voltage-dependent K^+ current (I; *lower*). *B*: summary plot of average peak K^+ current against step voltage shows an onset between −40 and −30 mV. *n* value indicates number of single neurons. *C*: using the same conditions as *A* (*inset*), a 1-Hz, 10-s train stimulus of the slow-phase ETP waveform (V; *upper*; in mV) evokes modest K^+ current (I; *lower*) in a neuron voltage-clamped at −40 mV. The K^+ current decreases over the time course; for clarity, only the response at 1 s (black) and 10 s (gray) are shown. *D*: plot of mean relative peak K^+ current during the slow-phase ETP waveform train stimulus reveals rapid run down, with a significant difference in current elicited by waveform 2 through 10 compared with 1 ($F_{9,162} = 19.358$, $P < 0.0001$, repeated-measures one-way ANOVA; $^*P < 0.01$ for 2–10 s, Dunnett multiple comparisons test). *n* value indicates number of single neurons. *E*: dual recording from coupled bag cell neurons in normal artificial seawater (nASW), with *neuron 1* voltage-clamped at –40 mV using K^+-Asp-based intracellular saline and *neuron 2* current-clamped (CC) to −40 mV with bias current, also using K^+-Asp but containing 71.25 mM tetraethylammonium (TEA) to partially block postsynaptic K^+ current (*inset*). Applying a 1-Hz, 10-s train stimulus of slow-phase action potential-like waveforms to *neuron 1* (V1; *upper*; in mV) elicits ETPs in *neuron 2* (V2, *lower*). The ETP changes little over the time; for clarity, only the response at 1 s (black) and 10 s (gray) is shown. *F*: summary plot of average relative peak ETP during the slow-phase action potential-like train stimulus shows that the response remains stable in the presence of postsynaptic TEA ($F_{9,27} = 0.6336$, $P = 0.7585$, repeated-measures one-way ANOVA). *n* value indicates number of pairs.

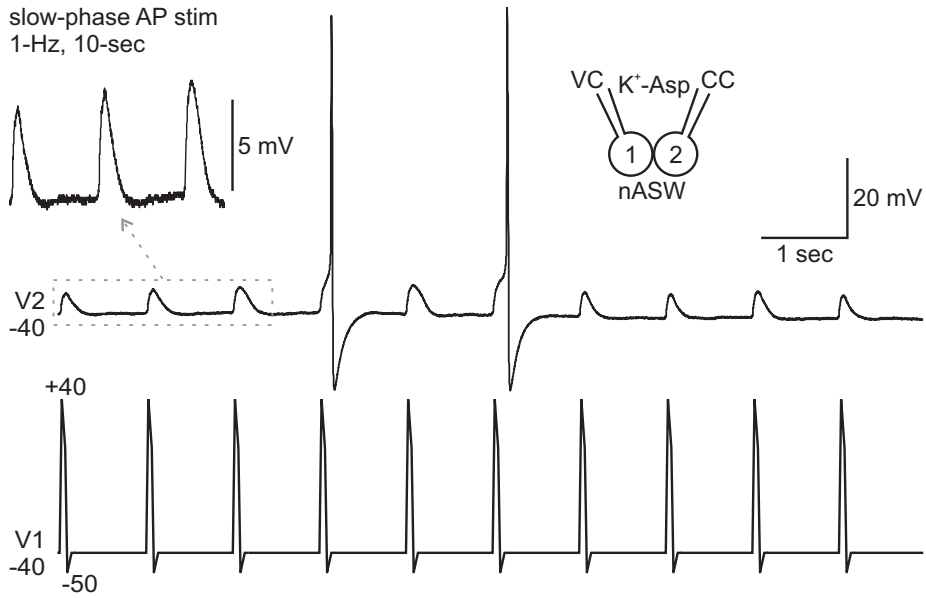

Figure 9. Repetitive presynaptic stimulation can cause postsynaptic spiking. A bag cell neuron pair recorded using K^+-Asp-based intracellular saline and normal artificial seawater (nASW) external saline (*inset*). *Neuron 1* is voltage-clamped (VC) at −40 mV while *neuron 2* is current-clamped (CC) to −40 mV using bias current. Delivery of the 1-Hz, 10-s train stimulus (stim) of slow-phase action potential (AP)-like waveforms to *neuron 1* (V1) evokes an electrotonic potential (ETP) in *neuron 2* (V2) that facilitates and eventually causes two spikes. Dashed box expanded on *upper left* shows how the first three ETPs facilitate by ∼20%. Representative of n = 6 pairs. Abscissa applies to both traces. Note that the ETPs following the action potentials in *neuron 2* fail to show consistent facilitation. We do not routinely observe interruptions to the upward trend of the ETP amplitude during the slow-phase train stimulus. However, given that voltage-gated Ca^{2+} influx can inhibit the bag cell neuron gap junction (39), it is possible the more substantial Ca^{2+} elevation during postsynaptic spiking transiently inhibits junctional conductance and disrupts ETP facilitation in this specific pair.

Facilitation of the ETP Serves to Drive and Maintain Synchronous Firing

Last, we sought to address whether use-dependent ETP facilitation has a role in feedforward excitation. The latter was apparent in our initial observations on the effects of the action potential-like waveforms presented in Fig. 4. Specifically, there were six additional pairs where the presynaptic slow-phase action potential-like waveform train stimulus caused postsynaptic spiking (Fig. 9). The mean number of action potentials elicited in *neuron 2* was 2.3 ± 0.80 (n = 6). For each of these particular pairs, the first few presynaptic waveforms evoked ETPs that facilitated from the start and eventually lead to postsynaptic spikes (Fig. 9, *dashed box*). On account of the action potentials in *neuron 2*, these pairs were not included in the summary data of Fig. 4*C*.

During the afterdischarge, firing is largely synchronous when most bag cell neurons are brought to threshold (22, 25). Although gap junctions are necessary for electrotonic spread of excitation through the network of the intact cluster (29), it is not clear if use-dependent facilitation occurs during synchronized firing. Thus, pairs of cultured coupled bag cell neurons were made to spike synchronously by transient exposure to acetylcholine, the input transmitter that initiates the afterdischarge through the opening of a monovalent cation-selective ligand-gated channel (24, 57). Initially, the timing and kinetics of the transmitter response were confirmed by pressure-ejecting 1 mM acetylcholine for 2 s simultaneously over the somata of both neurons in nASW while voltage-clamping with K^+-Asp-based intracellular saline (see METHODS, *Recording Conditions, Drug Application, and Reagents* for details). This elicited dual rapid-onset inward currents characteristic of ionotropic acetylcholine receptor activation (n = 4 pairs) (Fig. 10*A*), which were essentially identical to what we have published for single neurons (24, 58). The average acetylcholine-induced current was ∼−4 nA and not significantly different between *neurons 1* and *2* (Fig. 10*A*, *lower inset*); in addition, both currents consistently returned to baseline within ∼1 min.

Subsequently, different electrically coupled pairs were recorded in the same manner, except both neurons were under current-clamp. To further mimic conditions of the afterdischarge, protein kinase C was triggered with 100 nM phorbol 12-myristate 13-acetate (PMA) (59) ∼20 min before recording. The protein kinase C activity of intact clusters is elevated early in the slow phase and serves to enhance excitability by potentiating voltage-gated Ca^{2+} and nonselective cation channels, as well as increase junctional conductance (40, 46, 49, 60, 61), although it does not impact the amplitude or kinetics of the acetylcholine-induced current (56). With both neurons initially set to −40 mV in PMA, acetylcholine quickly evoked simultaneous depolarization and action potential firing (n = 10 pairs) (Fig. 10*B*). The bursts lasted ∼1 min (Fig. 10*D*, *left*) and were synchronous, with most spikes being phase-locked and yielding an average *neuron 1* to *neuron 2* cross-correlation estimate of ∼0.6 (Fig. 10*D*, *right*). Notably, in 5 of the 10 pairs, the one-to-one firing temporarily stopped, with just one of the neurons continuing to spike. For those cases, action potentials from the still-firing neuron induced facilitating ETPs that eventually renewed spiking in the other cell (Fig. 10*B*, *dashed box* and Fig. 10*C*); this typically required 5–10 s, although could happen in <2 s.

Recruitment back to synchrony occurred well past the ∼1 min recovery-time presented by the acetylcholine-induced current (compare Fig. 10*A* and Fig. 10*B*); nevertheless, it is possible that some persistent effect of acetylcholine or the continued presence of PMA (PKC activation) directly influenced the outcome. As an alternative, we attempted to drive use-dependent facilitation and feedforward excitation in untreated neurons. In current-clamped electrically coupled pairs, the *neuron 2* membrane potential was initially set just below the firing threshold, then a burst of spikes was elicited in *neuron 1* by a 5-s current step between 0.5 and 1 nA (n = 8). In these circumstances, there was moderate but clear feedforward excitation from *neuron 1* to *neuron 2*, with 32 ± 17% of the presynaptic action potentials transferring to the

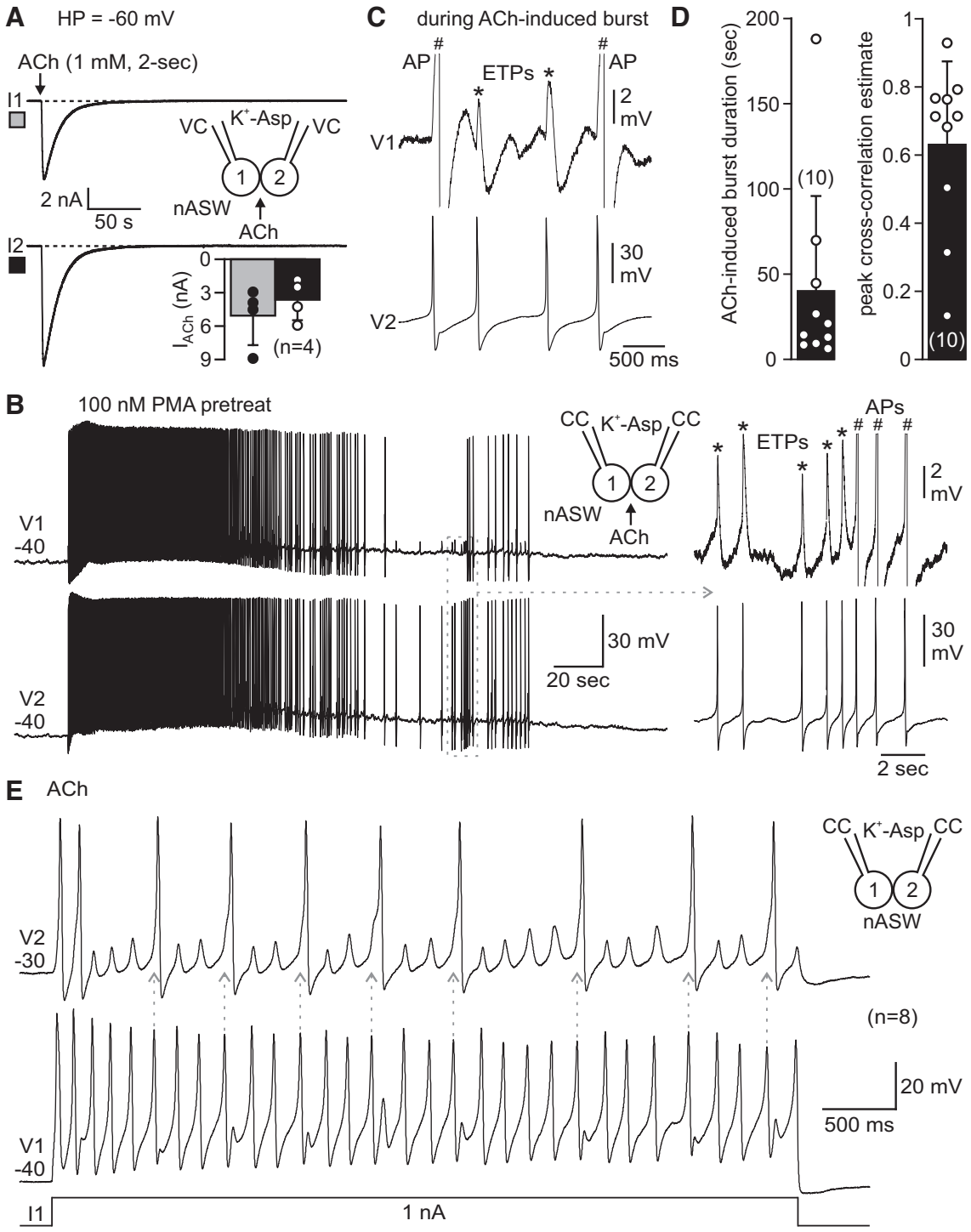

postsynaptic cell (Fig. 10*E*). Moreover, those postsynaptic spikes were preceded by ETPs that facilitated in a use-dependent manner and caused *neuron 2* to fire.

DISCUSSION

Electrical coupling between bag cell neurons is necessary for transforming an initial cholinergic input into a synchronized and spatially distributed afterdischarge that leads to egg-laying hormone secretion (24, 29, 62). In the pond snail, *Lymnaea stagnalis*, electrical synapses are also found between the homologous caudodorsal cells, which release reproductive hormones through a similar period of spiking (63, 64). Rat hypothalamic magnocellular neuroendocrine cells use electrical transmission to coordinate bursting and the secretion of oxytocin necessary for lactation and parturition (32, 65–67). The present study indicates that electrical transmission between bag cell neurons can facilitate during

modest firing, i.e., a slow-phase-like 1 Hz, which may support synchronous activity.

Within the cluster, paired recordings find coupling between both physically distant and adjacent bag cell neurons (25, 29). Accordingly, ultrastructural analysis of the cluster reveals gap junction arrays between the lengthy axons extending from somata as well as on an arrangement of small (1–3 μm) processes that separate juxtaposed somata (45). Thus, the soma-soma configuration employed here may reflect a connection that exists in the animal. Consistent with the electrical transmission, the cultured bag cell neuron synapse passes positive or negative current with little delay. However, the peak-to-peak action potential-to-ETP latency of bag cell neuron electrical transmission is slowed by the time required to charge the sizable (hundreds of pF) postsynaptic capacitance. Furthermore, low-pass filtering by the parallel combination of postsynaptic resistance and capacitance attenuates rapid presynaptic action potentials or action-potential-like waveforms. As such, most bag cell neuron ETPs have a monophasic recovery, rather than being biphasic, such as a spikelet observed in some coupled cortical interneurons that mimic the presynaptic waveform (68, 69).

All mammalian connexins close to one extent or another when the transjunctional voltage is made negative or positive (70). However, like various *Aplysia* and *Lymnaea* neurons (71–73), bag cell neuron junctional current is voltage-independent between −90 and 0 mV. This could explain why the coupling coefficient is constant with increasing hyperpolarization, despite anomalous rectification of the presynaptic membrane potential. The latter may be the result of an inwardly rectifying K^+ current, originally described by Kauer et al. (74). Because bag cell neurons are generally homogenous (22), coupled partners would have a similar membrane time constant; thus, even when anomalous rectification restricts presynaptic hyperpolarization, that voltage is faithfully transferred to the postsynaptic cell.

Regarding the facilitation of the bag cell neuron ETP, our results are in keeping with a progressive, low-amplitude, subthreshold effect of the ETP on the postsynaptic K^+ current, rather than an alteration to the gap junction itself. First, the junctional current between pairs remains stable over the course of a presynaptic slow-phase action potential-like waveform train stimulus. Second, injecting a junctional-like current train stimulus into individual neurons elicits facilitating ETP-like depolarizations. Third, delivering an ETP-like waveform train stimulus, again to single cells but isolating for Ca^{2+} channels, results in voltage-gated Ca^{2+} current that runs down slightly. Fourth, that same train stimulus given to individual neurons under conditions to record K^+ channels yields a cumulatively inactivating voltage-gated K^+ current. Fifth, blocking postsynaptic K^+ current before presynaptic stimulation with the slow-phase action potential-like waveform train stimulus impedes facilitation.

The use-dependent run-down of K^+ current is reminiscent of that reported for bag cell neurons by others (53, 56) and ourselves (54), as assayed with repeated steps to +20 or +30 mV. In the present study, the stimulus voltage is more limited, with the ETP-like waveform peaking at −19 mV. Even so, the K^+ current that does flow would oppose depolarization during a genuine ETP, while cumulative inactivation would lessen such a countering effect, thereby leading to facilitation. When intracellular TEA is added to the postsynaptic neuron, the K^+ current is proactively inhibited, so even if it changes further during the train stimulus, the impact on the ETP is likely limited. The small drop in Ca^{2+} current is anticipated to be less consequential, given that a reduction in inward current would not boost the ETP. Low-pass filtering could also promote cumulative inactivation of K^+ current by extending the postsynaptic voltage response, more so for the slow-phase waveform given its larger ETP area. This might be one reason why, during the fast-phase action potential-like waveform train stimulus, the electrical transmission fails to meaningfully facilitate, save for the somewhat inexplicable (perhaps by chance) increase of the 31st and 50th ETP. By sufficiently activating the K^+ current to cause some cumulative inactivation, the 1 Hz frequency of the slow-phase train stimulus seems better suited for facilitation.

For electrical transmission in other preparations, the ETP can engage postsynaptic conductances, typically subthreshold or persistent Na^+ current, such as in cerebellar (75), Mauthner (76), thalamic (77), trigeminal (78), or *Aplysia* buccal (8) neurons. Still, activity-dependent potentiation most often centers on tetanus-induced Ca^{2+} influx, through presynaptic or postsynaptic voltage-gated Ca^{2+} channels or postsynaptic ionotropic receptors, which may act through calmodulin kinase. At inferior olive neuron and Mauthner cell electrical synapses, the ETP or coupling coefficient is larger after stimulation (14, 79, 80), while the junctional current/conductance itself goes up at Retzius cell and thalamic neuron connections posttetanus (11, 12). Notably, the

Figure 10. Afterdischarge-like bursting in coupled neurons is synchronized. *A*: a pair of coupled bag cell neurons in normal artificial seawater (nASW) are voltage-clamped (VC) at −60 mV using K^+-Asp-based intracellular saline while acetylcholine (ACh) is pressure-ejected onto both cells (*upper inset*). Delivery of 1 mM acetylcholine for 2 s (at *arrow*) promptly induces inward current in both neurons (I1 and I2) with a rapid peak that recovers fully in <1 min. Scale bars apply to both traces. *Lower inset*, summary data of cholinergic current indicates no significant difference in mean peak amplitude in *neuron 1* (gray bar) vs. 2 (black bar) (t_3 = 0.6946, P = 0.5371; paired Student's t test). n value indicates number of pairs. *B*: coupled bag cell neurons under current-clamped (CC; *inset*) at −40 mV with bias current following ∼20 min pretreatment with 100 nM phorbol 12-myristate 13-acetate (PMA). Pressure ejection of 1 mM acetylcholine elicits depolarization and synchronous firing in both cells (V1 and V2). Scale bars apply to both traces. Dashed box expanded on the *right* reveals how at ∼2.5 min into the burst, when synchrony temporarily stops, a series of ∼1-Hz spikes in *neuron 2* evokes facilitating electrotonic potentials [ETPs; marked by asterisks (*)] that leads to resumed firing of action potentials [APs; marked by octothorpes (#); truncated top and bottom for clarity] in *neuron 1*. Abscissa applies to both traces. *C*: a separate pair of coupled neurons current-clamped under the same conditions as *B*. At the ∼12 s mark of an acetylcholine-induced burst, ∼1-Hz spikes in *neuron 2* (V2; *lower*) elicit facilitating ETPs followed by the restart of firing in *neuron 1* (V1; *upper*); action potentials truncated for clarity. Abscissa applies to both traces. *D*: mean burst duration evoked by acetylcholine (*left*). The degree of synchrony during the burst is reflected by a high average cross-correlation estimate (*right*). Number in bars is n-value that indicates number of pairs. *E*: a different coupled pair, in nASW alone, where bias current is used to current-clamp *neuron 1* (V1; *middle*) to below threshold at −40 mV and *neuron 2* (V2; *upper*) to near threshold at −30 mV. Injecting a 5-s, 1-nA depolarizing current into *neuron 1* (I1; *lower*) generates a burst of spikes that elicits concomitant phase-locked action potentials in *neuron 2* (gray arrows). After two postsynaptic spikes at the start of step, subsequent facilitating ETPs repeatedly summate to cause recurring firing in *neuron 2*. Representative of n = 8 pairs. Scale bars apply to both traces.

potentiation of electrical synapses in the thalamus raises the probability of feedforward excitation (12).

Facilitation of bag cell neuron electrical transmission is qualitatively similar to short-term potentiation of chemical transmission (10) but appears to be entirely a postsynaptic phenomenon (81). A parallel example of activity-dependent changes to the postsynaptic membrane influencing electrical coupling is found in *Aplysia* ink-gland motor neurons. These are three, electrically coupled cells that receive a common excitatory chemical synaptic input, with both a fast and slow component (82, 83). The slow component is due to a decrease in postsynaptic conductance, which effectively increases the input resistance of the motor neurons, enhances electrotonic coupling, and renders them more responsive to the inking motor program (83). Unlike in bag cell neurons, electrical coupling between ink-gland motor neurons does not appear to undergo use-dependent facilitation; rather, the decrease-conductance chemical input augments excitability and coupling, thus ensuring a synchronous burst. For bag cell neurons in the intact nervous system, Haskins and Blankenship (30) reported that trains of spikes originating in one cluster, due to stimulation or an afterdischarge, would propagate to the other cluster and evoke potentiating ETPs. They suggested that one cluster could act as a bursting pacemaker and drive activity in the other cluster through propagation and potentiation. The activity-dependent facilitation we describe here is a possible contributing factor to the potentiation documented by Haskins and Blankenship (30).

Coupled bag cell neurons synchronize when simultaneously driven to sustained spiking by acetylcholine in the presence of the PKC activator, PMA. This recapitulates observations in the intact cluster, where paired/multiple recordings show the neurons fire in unison during an afterdischarge (22, 29, 31). Electrically connected thalamic or trigeminal neurons will similarly synchronize when made to collectively spike by current injection (78, 84). Modeling also suggests that the introduction of coupling between independently firing neurons leads to coordinated activity and even the emergence of bursting from tonic spiking (85, 86). For bag cell neurons, use-dependent facilitation of electrical transmission can bring about feedforward excitation when either the slow-phase action potential-like waveform train stimulus or a tonic burst of genuine spikes is delivered presynaptically, as well as when both neurons are induced to spike with acetylcholine. In the latter instance, if one cell ceases to fire, action potentials in the other cell, occurring conspicuously at a slow-phase-like frequency, bring about facilitating ETPs that eventually rerecruit the silent neuron. Considering the slow phase makes up the bulk of the afterdischarge, this mechanism could guarantee any neurons that drop out as the response progresses are re-excited and continue to secrete reproductive hormones.

DATA AVAILABILITY

Data will be made available upon reasonable request.

ACKNOWLEDGMENTS

The authors thank CA London and HM Hodgson for technical assistance, as well as NM Magoski for the critical evaluation of previous drafts of the manuscript.

GRANTS

This study is supported by a Natural Sciences and Engineering Research Council of Canada Discovery Grant RGPI-2015-04G95 (to N.S.M.).

DISCLOSURES

No conflicts of interest, financial or otherwise, are declared by the authors.

AUTHOR CONTRIBUTIONS

N.S.M. conceived and designed research; Y.G. and A.B.P. performed experiments; Y.G., K.H.L., and N.S.M. analyzed data; Y.G. and N.S.M. interpreted results of experiments; Y.G., K.H.L., and N.S.M. prepared figures; K.H.L. and N.S.M. drafted manuscript; K.H.L. and N.S.M. edited and revised manuscript; K.H.L. and N.S.M. approved final version of manuscript.

REFERENCES

1. **Dahl G**, **Miller T**, **Paul D**, **Voellmy R**, **Werner R.** Expression of functional cell-cell channels from cloned rat liver gap junction complementary DNA. *Science* 236: 1290–1293, 1987. doi:10.1126/science.3035715.
2. **Phelan P**, **Stebbings LA**, **Baines RA**, **Bacon JP**, **Davies JA**, **Ford C.** Drosophila Shaking-B protein forms gap junctions in paired Xenopus oocytes. *Nature* 391: 181–184, 1998. doi:10.1038/34426.
3. **Phelan P**, **Bacon JP**, **Davies JA**, **Stebbings LA**, **Todman MG**, **Avery L**, **Baines RA**, **Barnes TM**, **Ford C**, **Hekimi S**, **Lee R**, **Shaw JE**, **Starich TA**, **Curtin KD**, **Sun YA**, **Wyman RJ.** Innexins: a family of invertebrate gap-junction proteins. *Trends Genet* 14: 348–349, 1998. doi:10.1016/s0168-9525(98)01547-9.
4. **Furshpan EJ**, **Potter DD.** Transmission at the giant motor synapses of the crayfish. *J Physiol* 145: 289–325, 1959. doi:10.1113/jphysiol.1959.sp006143.
5. **Bennett MVL**, **Zukin RS.** Electrical coupling and neuronal synchronization in the mammalian brain. *Neuron* 41: 495–511, 2004. doi:10.1016/s0896-6273(04)00043-1.
6. **Harris AL.** Electrical coupling and its channels. *J Gen Physiol* 150: 1606–1639, 2018. doi:10.1085/jgp.201812203.
7. **Regehr WG.** Short-term presynaptic plasticity. *Cold Spring Harb Perspect Biol* 4: a005702, 2012. doi:10.1101/cshperspect.a005702.
8. **Susswein AJ**, **Hurwitz I**, **Thorne R**, **Byrne JH**, **Baxter DA.** Mechanisms underlying fictive feeding in *Aplysia*: coupling between a large neuron with plateau potentials activity and a spiking neuron. *J Neurophysiol* 87: 2307–2323, 2002. doi:10.1152/jn.2002.87.5.2307.
9. **Nicoll RA.** A brief history of long-term potentiation. *Neuron* 93: 281–290, 2017. doi:10.1016/j.neuron.2016.12.015.
10. **Jackman SL**, **Regehr WG.** The mechanisms and functions of synaptic facilitation. *Neuron* 94: 447–464, 2017. doi:10.1016/j.neuron.2017.02.047.
11. **Welzel G**, **Schuster S.** Long-term potentiation in an innexin-based electrical synapse. *Sci Rep* 8: 12579, 2018. doi:10.1038/s41598-018-30966-w.
12. **Fricker B**, **Heckman E**, **Cunningham PC**, **Wang H**, **Haas JS.** Activity-dependent long-term potentiation of electrical synapses in the mammalian thalamus. *J Neurophysiol* 125: 476–488, 2021. doi:10.1152/jn.00471.2020.
13. **del Corsso C**, **Iglesias R**, **Zoidl G**, **Dermietzel R**, **Spray DC.** Calmodulin dependent protein kinase increases conductance at gap junctions formed by the neuronal gap junction protein connexin36. *Brain Res* 1487: 69–77, 2012. doi:10.1016/j.brainres.2012.06.058.
14. **Yang XD**, **Korn H**, **Faber DS.** Long-term potentiation of electrotonic coupling at mixed synapses. *Nature* 348: 542–545, 1990. doi:10.1038/348542a0.
15. **Eccles JC**, **Katz B**, **Kuffler SW.** Nature of the ''endplate potential'' in curarized muscle. *J Neurophysiol* 4: 362–387, 1941. doi:10.1152/jn.1941.4.5.362.
16. **Dudel J**, **Kuffler SW.** Mechanism of facilitation at the crayfish neuromuscular junction. *J Physiol* 155: 530–542, 1961. doi:10.1113/jphysiol.1961.sp006645.

17. **Charlton MP**, **Bittner GD.** Presynaptic potentials and facilitation of transmitter release in the squid giant synapse. *J Gen Physiol* 72: 487–511, 1978. doi:10.1085/jgp.72.4.487.
18. **Kupfermann I.** Stimulation of egg laying: possible neuroendocrine function of bag cells of abdominal ganglion of *Aplysia californica*. *Nature* 216: 814–815, 1967. doi:10.1038/216814a0.
19. **Arch S.** Polypeptide secretion from the isolated parietovisceral ganglion of *Aplysia californica*. *J Gen Physiol* 59: 47–59, 1972. doi:10.1085/jgp.59.1.47.
20. **Sturgeon RM**, **Chauhan AK**, **Magoski NS.** Neuroendocrine control of reproduction in *Aplysia* by the bag cell neurons. In: *Model Animals in Neuroendocrinology: From Worm to Mouse to Man*, edited by Ludwig M, Levkowitz G. Hoboken, NJ: Wiley, 2018, p. 29–58.
21. **Frazier WT**, **Kandel ER**, **Kupfermann I**, **Waziri R**, **Coggeshall RE.** Morphological and functional properties of identified neurons in the abdominal ganglion of *Aplysia californica*. *J Neurophysiol* 30: 1288–1351, 1967. doi:10.1152/jn.1967.30.6.1288.
22. **Kupfermann I**, **Kandel ER.** Electrophysiological properties and functional interconnections of two symmetrical neurosecretory clusters (bag cells) in abdominal ganglion of *Aplysia*. *J Neurophysiol* 33: 865–876, 1970. doi:10.1152/jn.1970.33.6.865.
23. **Kaczmarek LK**, **Jennings K**, **Strumwasser F.** An early sodium and a late calcium phase in the afterdischarge of peptide-secreting neurons of *Aplysia*. *Brain Res* 238: 105–115, 1982. doi:10.1016/0006-8993(82)90774-0.
24. **White SH**, **Magoski NS.** Acetylcholine-evoked afterdischarge in *Aplysia* bag cell neurons. *J Neurophysiol* 107: 2672–2685, 2012. doi:10.1152/jn.00745.2011.
25. **Blankenship J**, **Haskins J.** Electrotonic coupling among neuro-endocrine cells in *Aplysia*. *J Neurophysiol* 42: 347–355, 1979. doi:10.1152/jn.1979.42.2.347.
26. **Haskins JT**, **Price CH**, **Blankenship JE.** A light and electron microscopic investigation of the neurosecretory bag cells of *Aplysia*. *J Neurocytol* 10: 729–747, 1981. doi:10.1007/BF01262650.
27. **Michel S**, **Wayne NL.** Neurohormone secretion persists after post-afterdischarge membrane depolarization and cytosolic calcium elevation in peptidergic neurons in intact nervous tissue. *J Neurosci* 22: 9063–9069, 2002. doi:10.1523/JNEUROSCI.22-20-09063.2002.
28. **Hatcher NG**, **Sweedler JV.** *Aplysia* bag cells function as a distributed neurosecretory network. *J Neurophysiol* 99: 333–343, 2008. doi:10.1152/jn.00968.2007.
29. **Dargaei Z**, **Colmers PLW**, **Hodgson HM**, **Magoski NS.** Electrical coupling between *Aplysia* bag cell neurons: characterization and role in synchronous firing. *J Neurophysiol* 112: 2680–2696, 2014. doi:10.1152/jn.00494.2014.
30. **Haskins JT**, **Blankenship JE.** Interactions between bilateral clusters of neuroendocrine cells in *Aplysia*. *J Neurophysiol* 42: 356–367, 1979. doi:10.1152/jn.1979.42.2.356.
31. **Brown RO**, **Mayeri E.** Positive feedback by autoexcitatory neuropeptides in neuroendocrine bag cells of *Aplysia*. *J Neurosci* 9: 1443–1451, 1989. doi:10.1523/JNEUROSCI.09-04-01443.1989.
32. **Belin V**, **Moos F.** Paired recordings from supraoptic and paraventricular oxytocin cells in suckled rats: recruitment and synchronization. *J Physiol* 377: 369–390, 1986. doi:10.1113/jphysiol.1986.sp016192.
33. **Martin AO**, **Mathieu M-N**, **Chevillard C**, **Guerineau NC.** Gap junctions mediate electrical signalling and ensuing cytosolic Ca^{2+} increases between chromaffin cells in adrenal slices: a role in catecholamine release. *J Neurosci* 21: 5397–5405, 2001. doi:10.1523/JNEUROSCI.21-15-05397.2001.
34. **Ma Y**, **Juntti SA**, **Hu CK**, **Huguenard JR**, **Fernald RD.** Electrical synapses connect a network of gonadotropin releasing hormone neurons in a cichlid fish. *Proc Natl Acad Sci USA* 112: 3805–3810, 2015. doi:10.1073/pnas.1421851112.
35. **Hamill OP**, **Marty A**, **Neher E**, **Sakmann B**, **Sigworth FJ.** Improved patch-clamp techniques for high-resolution current recording from cells and cell-free membrane patches. *Pflugers Arch* 391: 85–100, 1981. doi:10.1007/BF00656997.
36. **Loechner KJ**, **Knox RJ**, **Connor JA**, **Kaczmarek LK.** Hyperosmotic media inhibit voltage-dependent calcium influx and peptide release in *Aplysia* neurons. *J Membr Biol* 128: 41–52, 1992. doi:10.1007/BF00231869.
37. **Fisher TE**, **Levy S**, **Kaczmarek LK.** Transient changes in intracellular calcium associated with a prolonged increase in excitability in neurons of *Aplysia californica*. *J Neurophysiol* 71: 1254–1257, 1994. doi:10.1152/jn.1994.71.3.1254.
38. **Magoski NS**, **Knox RJ**, **Kaczmarek LK.** Activation of a Ca^{2+}-permeable cation channel produces a prolonged attenuation of intracellular Ca^{2+} release in *Aplysia* bag cell neurones. *J Physiol* 522: 271–283, 2000. doi:10.1111/j.1469-7793.2000.t01-2-00271.x.
39. **Dargaei Z**, **Standage D**, **Groten CJ**, **Blohm G**, **Magoski NS.** Ca^{2+}-induced uncoupling of *Aplysia* bag cell neurons. *J Neurophysiol* 113: 808–821, 2015. doi:10.1152/jn.00603.2014.
40. **Beekharry CC**, **Gu Y**, **Magoski NS.** Protein kinase C enhances electrical synaptic transmission by acting on junctional and postsynaptic Ca^{2+} currents. *J Neurosci* 38: 2796–2808, 2018. doi:10.1523/JNEUROSCI.2619-17.2018.
41. **Li JZ**, **Magoski NS.** Electrical synapse location determines the strength of electrotonic transmission (Abstract). *Can Assoc Neurosci Abstr* 13: 1–48, 2019. https://can-acn.org/meeting-2019/2019-program/.
42. **Knox RJ**, **Jonas EA**, **Kao L-S**, **Smith PJS**, **Connor JA**, **Kaczmarek LK.** Ca^{2+} influx and activation of a cation current are coupled to intracellular Ca^{2+} release in peptidergic neurons of *Aplysia californica*. *J Physiol* 494: 627–639, 1996. doi:10.1113/jphysiol.1996.sp021520.
43. **Nick TA**, **Kaczmarek LK**, **Carew TJ.** Ionic currents underlying developmental regulation of repetitive firing in *Aplysia* bag cell neurons. *J Neurosci* 16: 7583–7598, 1996. doi:10.1523/JNEUROSCI.16-23-07583.1996.
44. **Chauhan-Puri AK**, **Lee KH**, **Magoski NS.** Hydrogen peroxide and phosphoinositide metabolites synergistically regulate a cation current to influence neuroendocrine cell bursting. *J Physiol* 599: 5281–5300, 2021. doi:10.1113/JP282302.
45. **Kaczmarek LK**, **Finbow M**, **Revel JR**, **Strumwasser F.** The morphology and coupling of *Aplysia* bag cells within the abdominal ganglion and in cell culture. *J Neurobiol* 10: 535–550, 1979. doi:10.1002/neu.480100604.
46. **Conn PJ**, **Strong JA**, **Kaczmarek LK.** Inhibitors of protein kinase C prevent enhancement of calcium current and action potentials in peptidergic neurons of *Aplysia*. *J Neurosci* 9: 480–487, 1989. doi:10.1523/JNEUROSCI.09-02-00480.1989.
47. **Sturgeon RM**, **Magoski NS.** Diacylglycerol-mediated regulation of *Aplysia* bag cell neuron excitability requires protein kinase C. *J Physiol* 594: 5573–5592, 2016. doi:10.1113/JP272152.
48. **Kaczmarek LK**, **Strumwasser F.** A voltage-clamp analysis of currents underlying cyclic AMP-induced membrane modulation in isolated peptidergic neurons of *Aplysia*. *J Neurophysiol* 52: 340–349, 1984. doi:10.1152/jn.1984.52.2.340.
49. **Tam AKH**, **Geiger JE**, **Hung AY**, **Groten CJ**, **Magoski NS.** Persistent Ca^{2+} current contributes to a prolonged depolarization in *Aplysia* bag cell neurons. *J Neurophysiol* 102: 3753–3765, 2009. doi:10.1152/jn.00669.2009.
50. **Hung AY**, **Magoski NS.** Activity-dependent initiation of a prolonged depolarization in *Aplysia* bag cell neurons: role for a cation channel. *J Neurophysiol* 97: 2465–2479, 2007. doi:10.1152/jn.00941.2006.
51. **Groten CJ**, **Magoski NS.** PKC enhances the capacity for secretion by rapidly recruiting covert voltage-gated Ca^{2+} channels to the membrane. *J Neurosci* 35: 2747–2765, 2015. doi:10.1523/JNEUROSCI.3581-14.2015.
52. **Strong JA.** Modulation of potassium current kinetics in bag cell neurons of *Aplysia* by an activator of adenylate cyclase. *J Neurosci* 4: 2772–2783, 1984. doi:10.1523/JNEUROSCI.04-11-02772.1984.
53. **Strong JA**, **Kaczmarek LK.** Multiple components of delayed potassium current in peptidergic neurons of *Aplysia*: modulation by an activator of adenylate cyclase. *J Neurosci* 6: 814–822, 1986. doi:10.1523/JNEUROSCI.06-03-00814.1986.
54. **White SH**, **Sturgeon RM**, **Magoski NS.** Nicotine inhibits potassium currents in *Aplysia* bag cell neurons. *J Neurophysiol* 115: 2635–2648, 2016. doi:10.1152/jn.00816.2015.
55. **De Nó RL.** On the effect of certain quaternary ammonium ions upon frog nerve. *J cell comp Physiol* 33: 167–231, 1949. doi:10.1002/jcp.1030330404.
56. **Quattrocki EA**, **Marshall J**, **Kaczmarek LK.** A Shab potassium channel contributes to action potential broadening in peptidergic neurons. *Neuron* 12: 73–86, 1994. doi:10.1016/0896-6273(94)90153-8.

57. **White SH**, **Carter CJ**, **Magoski NS.** A potentially novel nicotinic receptor in *Aplysia* neuroendocrine cells. *J Neurophysiol* 112: 446–462, 2014. doi:10.1152/jn.00796.2013.
58. **White SH**, **Sturgeon RM**, **Gu Y**, **Nensi A**, **Magoski NS.** Tyrosine phosphorylation determines afterdischarge initiation by regulating an ionotropic cholinergic receptor. *Neuroscience* 372: 273–288, 2018. doi:10.1016/j.neuroscience.2017.12.049.
59. **Castagna M**, **Takai Y**, **Kaibuchi K**, **Sano K**, **Kikkawa U**, **Nishizuka Y.** Direct activation of calcium-activated, phospholipid-dependent protein kinase by tumor-promoting phorbol esters. *J Biol Chem* 257: 7847–7851, 1982. doi:10.1016/S0021-9258(18)34459-4.
60. **Wilson GF**, **Magoski NS**, **Kaczmarek LK.** Modulation of a calcium-sensitive nonspecific cation channel by closely associated protein kinase and phosphatase activities. *Proc Natl Acad Sci USA* 95: 10938–10943, 1998. doi:10.1073/pnas.95.18.10938.
61. **Wayne NL**, **Lee W**, **Kim YJ.** Persistent activation of calcium-activated and calcium-independent protein kinase C in response to electrical afterdischarge from peptidergic neurons of *Aplysia*. *Brain Res* 834: 211–213, 1999. doi:10.1016/s0006-8993(99)01594-2.
62. **Pinsker HM**, **Dudek FE.** Bag cell control of egg laying in freely behaving *Aplysia*. *Science* 197: 490–493, 1977. doi:10.1126/science.197.4302.490.
63. **De Vlieger TA**, **Kits KS**, **Ter Maat A**, **Lodder JC.** Morphology and electrophysiology of the ovulation hormone producing neuro-endocrine cells of the freshwater snail Lymnaea stagnalis (L.). *J Exp Biol* 84: 259–271, 1980. doi:10.1242/jeb.84.1.259.
64. **Geraerts WPM**, **Tensen CP**, **Hogenes TM.** Multiple release of peptides by electrically active neurosecretory caudo-dorsal cells of *Lymnaea stagnalis*. *Neurosci Lett* 41: 151–155, 1983. doi:10.1016/0304-3940(83)90238-0.
65. **Lincoln DW**, **Wakerley JB.** Electrophysiological evidence for the activation of supraoptic neurones during the release of oxytocin. *J Physiol* 242: 533–554, 1974. doi:10.1113/jphysiol.1974.sp010722.
66. **Andrew RD**, **MacVicar BA**, **Dudek FE**, **Hatton GI.** Dye transfer through gap junctions between neuroendocrine cells of rat hypothalamus. *Science* 211: 1187–1189, 1981. doi:10.1126/science.7466393.
67. **Summerlee A.** Extracellular recordings from oxytocin neurones during the expulsive phase of birth in unaesthetized rats. *J Physiol* 321: 1–9, 1981. doi:10.1113/jphysiol.1981.sp013967.
68. **Galarreta M**, **Hestrin S.** A network of fast-spiking cells in the neocortex connected by electrical synapses. *Nature* 402: 72–75, 1999. doi:10.1038/47029.
69. **Zsiros V**, **Maccaferri G.** Noradrenergic modulation of electrical coupling in GABAergic networks of the hippocampus. *J Neurosci* 28: 1804–1815, 2008. doi:10.1523/JNEUROSCI.4616-07.2008.
70. **González D**, **Gómez-Hernández JM**, **Barrio LC.** Molecular basis of voltage dependence of connexin channels: an integrative appraisal. *Prog Biophys Mol Biol* 94: 66–106, 2007. doi:10.1016/j.pbiomolbio.2007.03.007.
71. **Bodmer R**, **Verselis V**, **Levitan IB**, **Spray DC.** Electrotonic synapses between *Aplysia* neurons in situ and in culture: aspects of regulation and measurements of permeability. *J Neurosci* 8: 1656–1670, 1988. doi:10.1523/JNEUROSCI.08-05-01656.1988.
72. **Carrow GM**, **Levitan IB.** Selective formation and modulation of electrical synapses between cultured *Aplysia* neurons. *J Neurosci* 9: 3657–3664, 1989. doi:10.1523/JNEUROSCI.09-10-03657.1989.
73. **Wildering WC**, **Janse C.** Serotonergic modulation of junctional conductance in an identified pair of neurons in the mollusc *Lymnaea stagnalis*. *Brain Res* 595: 343–352, 1992. doi:10.1016/0006-8993(92)91070-u.
74. **Kauer JA**, **Fisher TE**, **Kaczmarek LK.** Alpha bag cell peptide directly modulates the excitability of the neurons that release it. *J Neurosci* 7: 3623–3632, 1987. doi:10.1523/JNEUROSCI.07-11-03623.1987.
75. **Mann-Metzer P**, **Yarom Y.** Electrotonic coupling interacts with intrinsic properties to generate synchronized activity in cerebellar networks of inhibitory interneurons. *J Neurosci* 19: 3298–3306, 1999. doi:10.1523/JNEUROSCI.19-09-03298.1999.
76. **Curti S**, **Pereda AE.** Voltage-dependent enhancement of electrical coupling by a subthreshold sodium current. *J Neurosci* 24: 3999–4010, 2004. doi:10.1523/JNEUROSCI.0077-04.2004.
77. **Haas JS**, **Landisman CE.** State-dependent modulation of gap junction signaling by the persistent sodium current. *Front Cell Neurosci* 5: 31, 2011. doi:10.3389/fncel.2011.00031.
78. **Curti S**, **Hoge G**, **Nagy JI**, **Pereda AE.** Synergy between electrical coupling and membrane properties promotes strong synchronization of neurons of the mesencephalic trigeminal nucleus. *J Neurosci* 32: 4341–4359, 2012. doi:10.1523/JNEUROSCI.6216-11.2012.
79. **Turecek J**, **Yuen GS**, **Han VZ**, **Zeng XH**, **Bayer KU**, **Welsh JP.** NMDA receptor activation strengthens weak electrical coupling in mammalian brain. *Neuron* 81: 1375–1388, 2014. [Erratum in *Neuron* 82: 500, 2014]. doi:10.1016/j.neuron.2014.01.024.
80. **Pereda AE**, **Bell TD**, **Chang BH**, **Czernik AJ**, **Nairn AC**, **Soderling TR**, **Faber DS.** Ca^{2+}/calmodulin-dependent kinase II mediates simultaneous enhancement of gap-junctional conductance and glutamatergic transmission. *Proc Natl Acad Sci USA* 95: 13272–13277, 1998. doi:10.1073/pnas.95.22.13272.
81. **Alcamí P**, **Pereda AE.** Beyond plasticity: the dynamic impact of electrical synapses on neural circuits. *Nat Rev Neurosci* 20: 253–271, 2019. doi:10.1038/s41583-019-0133-5.
82. **Carew TJ**, **Kandel ER.** Inking in *Aplysia californica*. I. Neural circuit of an all-or-none behavioral response. *J Neurophysiol* 40: 692–707, 1977. doi:10.1152/jn.1977.40.3.692.
83. **Carew TJ**, **Kandel ER.** Inking in *Aplysia californica*. III. Two different synaptic conductance mechanisms for triggering central program for inking. *J Neurophysiol* 40: 721–734, 1977. doi:10.1152/jn.1977.40.3.721.
84. **Long MA**, **Landisman CE**, **Connors BW.** Small clusters of electrically coupled neurons generate synchronous rhythms in the thalamic reticular nucleus. *J Neurosci* 24: 341–349, 2004. doi:10.1523/JNEUROSCI.3358-03.2004.
85. **LeMasson G**, **Marder E**, **Abbott LF.** Activity-dependent regulation of conductances in model neurons. *Science* 259: 1915–1917, 1993. doi:10.1126/science.8456317.
86. **Horn KG**, **Memelli H**, **Solomon IC.** Emergent central pattern generator behavior in gap-junction-coupled Hodgkin–Huxley style neuron model. *Comput Intell Neurosci* 2012: 173910, 2012. doi:10.1155/2012/173910.